2015-01-01

Crustal Structure Beneath The Eastern Nepal Himalayas And Southern Tibet From Receiver Function Analysis

Arjun Sharma Neupane
University of Texas at El Paso, arjunneupane@gmail.com

CRUSTAL STRUCTURE BENEATH THE EASTERN NEPAL HIMALAYAS AND SOUTHERN TIBET FROM RECEIVER FUNCTION ANALYSIS

ARJUN SHARMA NEUPANE

Department of Physics

APPROVED:

Aaron A.Velasco, Ph.D., Chair

Tunna Baruah, Ph.D.

Rajendra Zope, Ph.D.

Charles Ambler, Ph.D.
Dean of the Graduate School

Dedication

To all the Nepalese people affected by the April 25th magnitude 7.8 earthquake

CRUSTAL STRUCTURE BENEATH THE EASTERN NEPAL HIMALAYAS AND SOUTHERN TIBET FROM RECEIVER FUNCTION ANALYSIS

by

ARJUN SHARMA NEUPANE, M.Sc.

THESIS

Presented to the Faculty of the Graduate School of

The University of Texas at El Paso

in Partial Fulfillment

of the Requirements

for the Degree of

MASTER OF SCIENCE

Department of Physics

THE UNIVERSITY OF TEXAS AT EL PASO

May 2015

Acknowledgements

I express my sincere thanks and gratitude to my adviser, Aaron Velasco, for his mentoring, guidance and encouragement during the past two years. His lectures and suggestions have been invaluable for me to build a platform in Seismology and to understand and implement the technical basics of research and writing. I wouldn't have been able to complete my project without his continuous support and guidance. I also thank other members of my thesis committee, Tunna Baruah and Rajendra Zope for their useful advice and insightful lectures.

I would also like to thank Mohan Pant for his part in this project and for being a wonderful friend. I extend my thanks also to Sanjaya Lohani for continuously reminding me the importance of mathematics and for his help and guidance in physics and mathematics.

My master's study is funded by the Department of Physics at UTEP. I am grateful to Vivian Incera for providing me the opportunity to study at UTEP. I am also grateful to Efrain Ferrer for his wonderful lectures in Quantum Mechanics and Statistical Mechanics. I also thank Carla Karmona for being a great lab supervisor and Alex Price for being a good friend.

Finally, I am grateful to my family for their unconditional love and support. I also thank Neeti Bashyal for being a source of motivation.

Abstract

The Himalayas are the results of continental collision between the Indian plate and the Eurasian plate and serve as a natural site to study the physical causes and process of mountain building. The crustal structure beneath the Himalayas has been subject to numerous geophysical studies and the variation in the velocity structure across the Himalayan region suggests significant differences in the crustal structure between the southern and northern portion in that region. In this research, a P receiver function analysis has been conducted on data collected for 14 years (2000-2014) from 211 different stations in Eastern Nepal and Southern Tibet, to better understand the seismic velocity structure in the region. The stations cover a large area encompassing the south eastern plains of Nepal, Lesser and Greater Himalayas and the Southern Tibetan Plateau and provide an excellent geometry for seismic structure research. Following the rotation of the two horizontal components to the radial and transverse components and the time iterative deconvolution to obtain the receiver functions the H-K stacking method of Zhu and Kanamori(Zhu and Kanamori, 2000) has been used to convert the time domain receiver functions into H-K domain and obtain the values of crustal thickness and the ratio of the P and S wave velocities. The main trend in the receiver function analysis across the Himalaya from our study reflects the deepening of the moho from about 40 km beneath southern Nepal in the foothills of the Himalaya to about 80 km in southern Tibet. A locally steeper moho deep is obtained in the high range of Himalayas.

Table of Contents

List of Tables

List of Figures

Chapter 1: Introduction

The Himalayan range result from the continental collision between the Indian and Eurasian Plates and is composed of detached slices of the crust of Indian Plate (Molnar, 1984) that underthrusts the mountain chain and the south Tibetan Plateau (Zhao et al., 1993). As a result of the underthrusting, the crust in the Himalayan range has been thickened across the collision zone, with differences in thickness greater than 30 km between southern Nepal and southern Tibet (Schulte-Pelkum et al., 2005). The collision of the Indian and Eurasian Plate provides a natural setting for the study of the physical and geological process involved in mountain building and the study of the crustal structure beneath that region provides invaluable information about the ongoing geomorphology, including the subduction of Indian Plate beneath the Eurasian Plate and the faulting structures in the Indian subcontinent. For example, the increase in upper mantle P wave velocity(V_P) from south to north of the Greater Himalayas might be the result of metamorphism of the rocks in the lower crust of the underthrusting Indian Plate to eclogite as they plunge into greater depth beneath the mountain range, as suggested by Monsalve et al. (2008).

In obtaining more insight of the underlying structure of the Himalayas, the crust and the lithosphere play major role in validating or disproving the current theories about the Himalayan collision zone. Several geophysical studies have been carried out to better understand and map the velocity contrast of the crust mantle boundary in the Eastern Himalayas and the adjoining regions among which receiver function analysis (Sheehan et al., 2002;Nábělek et al., 2009;Schulte-Pelkum et al., 2005), seismicity and 1 D velocity modeling (Monsalve et al., 2008;Velasco et al., 2007), surface wave dispersion (Gupta and Narain, 1967), INDEPTH reflection survey (Alsdorf et al., 1998), body waves study (Tandon and Dube, 1973). These

studies have provided useful information about overall crustal structure, moho depth and Poisson's ratio in a wide area covering the eastern and central Nepal, Southern Tibet and Bhutan.

Among different methods used to understand the crustal structure beneath the Himalayas, the receiver function method was found to be most sensitive in providing the value for moho depth. The receiver function technique (Langston, 1979; Ligorría and Ammon, 1999; Zhu and Kanamori, 2000) uses the travel times of P and P to S converted phases and other reverberations (multiples) to find an estimate of the moho depth and Vp/Vs ratio. To obtain an accurate estimate of the moho depth, the absolute crustal velocity is required which can be estimated by techniques such as the combined surface wave and receiver function analysis (Özalaybey et al., 1997). However, it is a common practice to assume an average value for the crustal velocity and the Poisson's ratio whenever the crustal velocity cannot be easily estimated.

The goal of this project is to image the crustal structure beneath the eastern Nepal Himalayas, southern Tibet and Bhutan using the *P* wave receiver function calculated from 211 temporary deployed and GSN seismic stations in the region. The values of moho depth V_P/V_S ratio are in agreement with the results of previous studies done in the similar region. In the following chapters, Chapter 2 describes the geological and tectonic setting of the study area. Chapter 3 provides the data and processing technique along with the detailed receiver function analysis. The results of the study are presented in Chapter 4. Chapter 5 consists of discussion of the results, comparison with the previous results and possible topics for further research.

Chapter 2: Geological and Tectonic Setting

2.1: INTRODUCTION

The Indian plate has been constantly colliding with the Eurasian plate for at least 40 million years. The great Himalayas and the Tibetan plateau are the results of the collision process and are considered as the one of the most spectacular and challenging geological features in the world. The convergence rate between India and Eurasia requires rapid slip rate and the occurrence of four great earthquakes with magnitude greater than 8.4 in the last 100 years attests to high seismic activity and a rapid rate of active deformation (Seeber et al., 1981)

Although the area of eastern Nepal, southern Tibet and Bhutan covered in this project reflects only a small portion of the whole Himalayan arc, some major geologic and tectonic features of the Himalayas associated with the Indian-Eurasian collision zone are briefly explained in this section. The Himalayan-Tibetan orogen may be subdivided into several individual blocks. The Himalayas can be divided into six primary lithotectonic zones which run as parallel belts. These zones include Trans-Himalayan batholith, Indus-Tsangpo suture zone, Tethyan(Tibetan) Himalaya, Higher(Greater) Himalaya, Lesser(Lower) Himalaya, and the Sub-Himalaya. Major focus is given to The Himalayan sequence which includes most of the Nepal Himalayas. Figure 2.1 shows the geological structure of the Himalayan-Tibet orogen.

2.2: MAJOR TECTONIC DIVISIONS

The Sub-Himalaya:

This Sub-Himalaya zone consists of clastic sediments that were produced by the uplift and subsequent erosion of the Himalayas and deposited by rivers. These rocks have been folded and

faulted to produce the Siwalik Hills that are at the foot of the great mountains (Sorkhabi and Macfarlane, 1999).. Sub-Himalayan rocks have been overthrust by the Lesser Himalayas along the Main Boundary Thrust Fault. This steep thrust flattens with depth, developed during the Pliocene time and has been shown as active through the Pleistocene. In turn, the Sub-Himalayas are bounded by a thrust fault to the south and are forced over sediments on the Indian plate. This fault system is called the Himalayan Frontal thrust (Sorkhabi and Macfarlane, 1999).

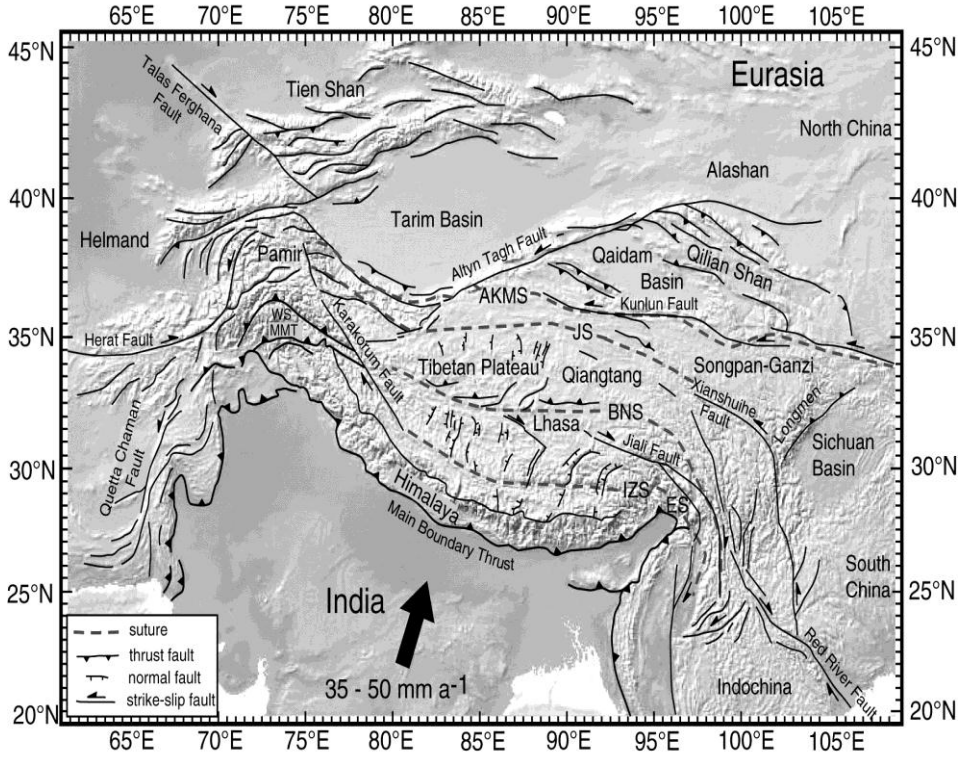

Figure 2.1: Himalayan-Tibetan orogen. WS - Western Himalayan Syntaxis; ES - Eastern Himalayan Syntaxis; MMT - Main Mantle Thrust; AKMS – Anyimaqen-Kunlun-Muztagh suture; JS - Jinsha Suture; BNS - Bangong-Nujiang Suture; IZS - Indus-Zangbo suture. From (Kearey et al., 2009)

Main Central Fault:

This thrust fault was first described by Heim and Gansser (Heim and Gansser, 1939) and marks the boundary between the higher and lesser Himalayan mountains. It is a longitudinal thrust fault, and in many places is marked by a several kilometer thick zone of deformed rocks with varying degrees of shearing and imbrication (Sorkhabi and Macfarlane, 1999). Movement along the fault has brought crystalline rock from the Higher Himalayan zone on top of Lesser Paleozoic sediments in the form of klippen in synclines (Windley, 1995). These units are called the Outer Crystallines, as noted above on the map. Outer crystalline rocks, garnet and kyanite-bearing, were exposed by slip along the MCT followed by uplift and erosion of 10km of overlying rock (Molnar, 1984). Figure 2.2 shows tectonic features of Nepal and adjoining region with major thrust fault systems.

Lesser Himalaya:

Bounded by the Main Central Thrust (MCT) in the north and Main Boundary Thrust (MBT) to the south, the lesser Himalayas only experienced up to greenschist facies metamorphism. They are primarily sedimentary rocks from the Indian platform. Rock units here also show a series of anticlines and synclines that are in many cases quite sheared. Fossils have been documented in this zone, but they do not occur as frequently as in Tehtyan zone in the north.

The Higher Himalaya:

This zone extends from the MCT to Tibetan-Tethys Zone and runs throughout Nepal. This zone consists of almost 10 km thick succession of the crystalline rocks which can be divided into four main units, as Kyanite-Sillimanite gneiss, pyroxenic marble and gneiss, banded gneiss, and augen gneiss in the ascending order.

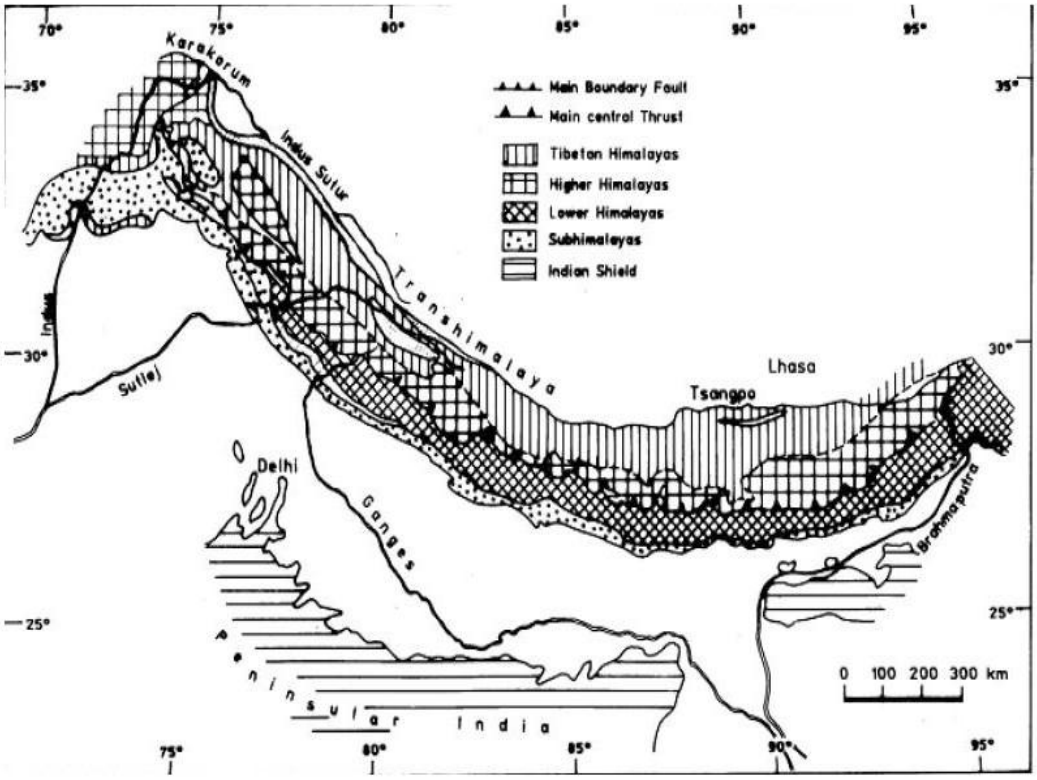

Figure 2.2: Tectonic map of Himalayas and adjoining areas showing major fault regions (Gansser, 1964)

Tethyan Himalaya:

The Tibetan-Tethys Himalayas generally begins from the top of the Higher Himalayan Zone and extends to the north in Tibet. In Nepal these fossiliferous rocks are well developed in Thak Khola (Mustang), Manang and Dolpa area (Liu and Einsele, 1994). This zone is about 40 km wide and composed of fossiliferous sedimentary rocks such as shale, sandstone and limestone etc. The area north of the Annapurna and Manaslu ranges in central Nepal consists of metasediments that overlie the Higher Himalayan zone along the South Tibetan Detachment

system. It has undergone very little metamorphism except at its base where it is close to the Higher Himalayan crystalline rocks. The thickness is currently presumed to be 7,400 m.). The rocks of the Tibetan Tethys Series (TSS) consist of a thick and nearly continuous lower Paleozoic to lower Tertiary marine sedimentary succession. The rocks are considered to be deposited in a part of the Indian passive continental margin (Liu and Einsele, 1994).

The other subdivisions of the Himalayan-Tibetan orogen include Indus-Tsangpo Suture Zone, Eastern Trans-Himalaya, Western Trans-Himalaya and Trans-Himalayan Batholith.

Chapter 3: Basic Seismology

Some basic terms in seismology are introduced in this section in order to have the foundation to understand receiver functions. The structure of earth has been studied for many years and the recordings of seismic signals has provided us the overall structure of the earth that we know of today. Figure 3.1 shows the internal structure of the earth illustrating different layers which are distinguished on the basis of chemical and physical properties.

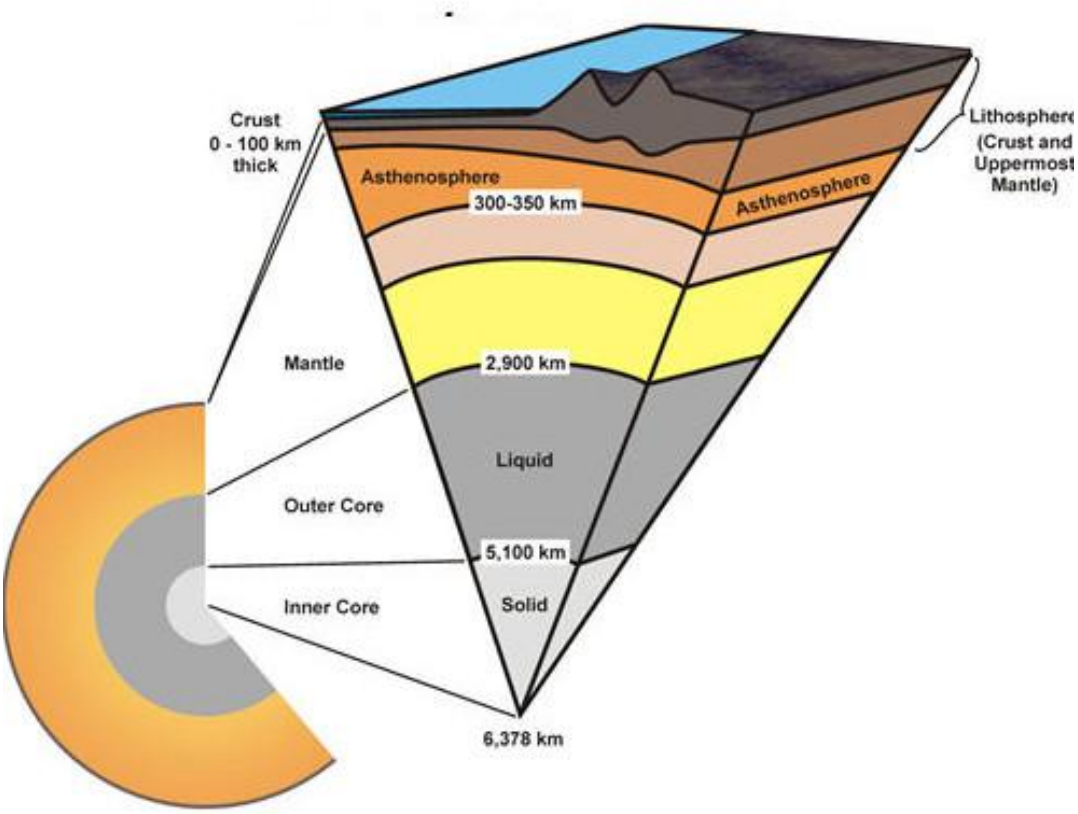

Figure 3.1: Division in interior of the Earth

The seismic discontinuity inside the earth helps to distinguish the layers of earth into crust (oceanic and continental), transition region, upper mantle, lower mantle, D", outer core and inner core. The boundary between crust and mantle is called moho, named after Croatian seismologist Andrija Mohorovičić who discovered an abrupt increase in seismic velocity while analyzing the seismic data for an earthquake. The moho region is very important in the context of this project as the receiver function method helps to find the moho depth. As the thickness of the crust varies the moho depth usually varies from 35-70kms beneath the continents and from 5-10 kms beneath the ocean.

Seismology is the study of earthquakes and seismic waves that move through and around the earth. When an earthquake occurs seismic waves are generated that transfer the energy throughout the interior of the earth and on the surface of the earth. The point where the earthquake occurs by the sudden release of energy that has been stored over time is called the hypocenter and the projection of that point on the surface of the earth is called as epicenter. There are two basic kinds of waves, namely, body waves and surface waves. The body waves are further classified as P wave, the primary wave and S wave, the secondary wave. The P wave, see Figure 3.2, like the sound wave, is a compressional pressure wave and is first to arrive at a seismic station. The P wave can move through solid rock and fluids, like water or the liquid layers of the earth. On the other hand the S wave, see Figure 2.2, is a shear wave, causing shearing deformation without the change in volume. The S wave is slower than the P wave and arrives next, shaking the ground up and down and back and forth perpendicular to the direction it is traveling. An S wave is slower than a P wave and can only move through solid rock, not through any liquid medium. The S waves are second to arrive to a seismic station and hence are called secondary waves.

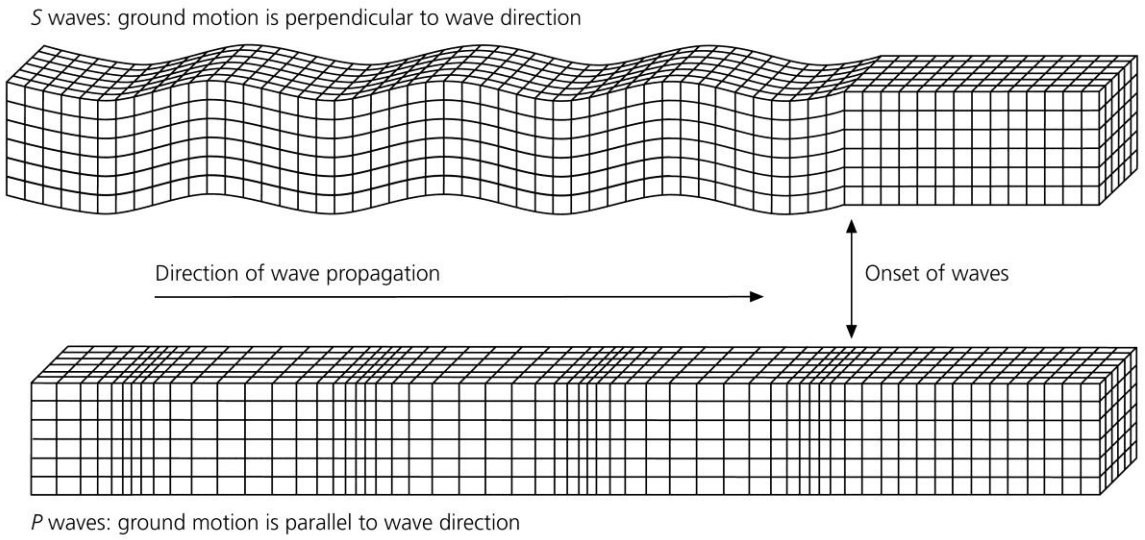

Figure 3.2: Diagrams of S and P waves adapted from (Stein and Wysession, 2002)

The other types of wave, Surface waves, travel only through the crust and have lower frequency than the body waves. Although they arrive after the body waves they produce more damage than the body waves during an earthquake. The surface waves are further classified as Love wave and Raleigh wave. Love waves, see Figure 3.3, are the first arriving surface waves with horizontal particle motion, which is perpendicular to direction of propagation (transverse). The other type of surface waves is called a Raleigh wave. The particle motion during the propagation of Raleigh waves consists of elliptical motion in the vertical plane and parallel to the direction of propagation. In both types of surface waves material returns to its original shape after the wave passes.

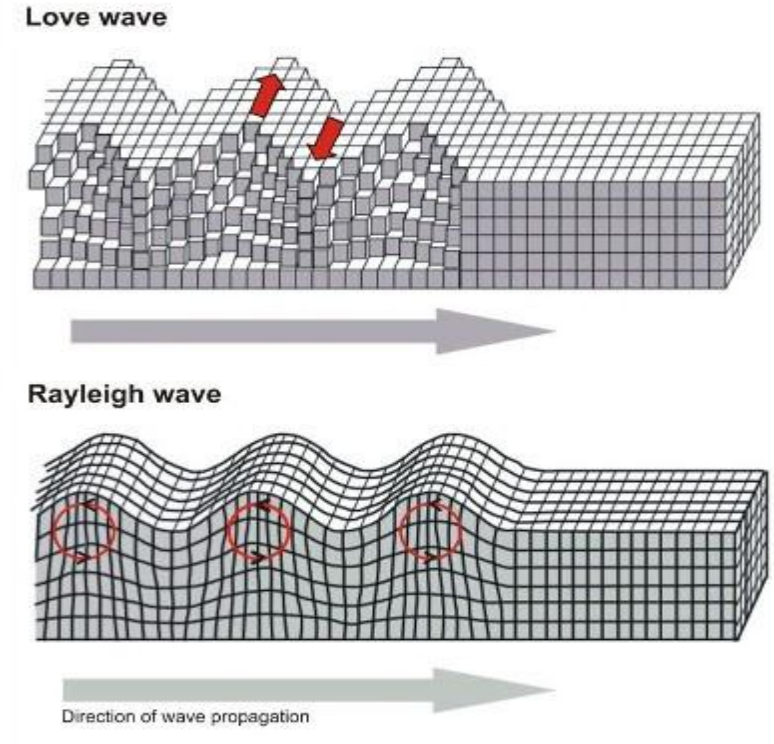

Figure3.3: Love wave and Rayleigh wave with particle motion directions

Seismic signals are recorded as a time series of the displacement of the earth. Such recording of a time series data is known as a seismogram, see Figure 3.4, which usually records the movement of earth in three directions, vertical Z, east-west EW and north-south NS. The recording on a seismogram may be due to an earthquake or from other sources of energy like an explosion and the ambient noises. Historically seismograms were recorded on a paper attached to the rotating drums, but, today practically all seismograms are recorded digitally to make the analysis by computer easier. Seismograms are essential for studying the earthquakes and the structure of earth.

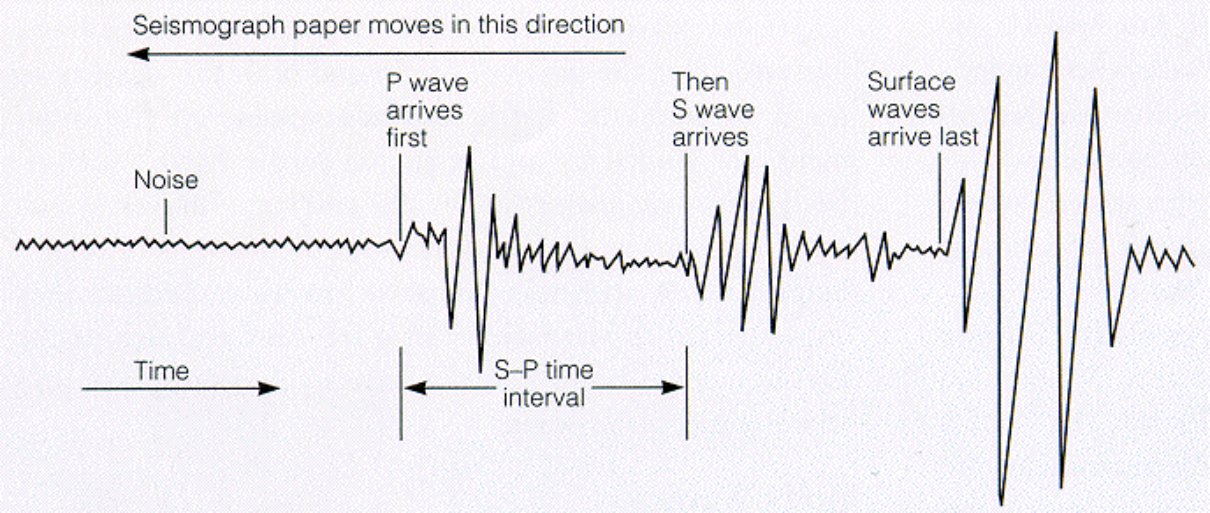

Figure 3.4: A typical seismogram recorded on a constantly moving paper. Today practically all seismogram are recorded digitally.

Earthquakes are classified into three categories on the basis of distance of the source to the seismograph station. The earthquakes recorded at a distance larger than 1000 km from the source are known as teleseismic events, see Figure 3.5. The wavefront of a teleseismic event is generally considered as a plane wave. Earthquakes recorded at a distance greater than 500 and less than 1000 km are known as regional events and the earthquakes for which the epicentral distance from the station is less than 500 km are known as local events.

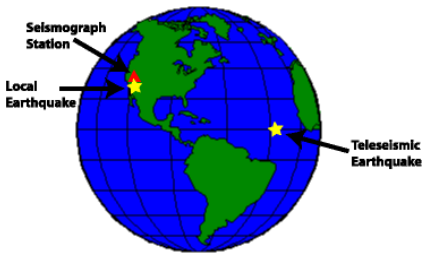

Figure3.5: Teleseismic and local events

Chapter 4: Data and Processing

4.1: DATA

The data used in this research are a very large number of events from 2000 to 2014 recorded at 226 seismic stations in the eastern Nepal, Northeastern India, Tibet and Bhutan area. Most of the stations are the part of GSN networks, while, few were temporary deployments carried out for number of years. The data was downloaded using a program called Standing Order for Data(SOD) freely provided by the department of geological science at the university of South Carolina and the IRIS consortium. The data were selected on the basis of following criteria: moment magnitude greater than 5.9, latitude between 25 and 35 degrees, longitude between 85.5 to 100 degrees. Figure 2.1 shows the locations of all the broadband seismic stations used in this research. The stations map is followed by Table 4.1 with the list of all the stations and their coordinates.

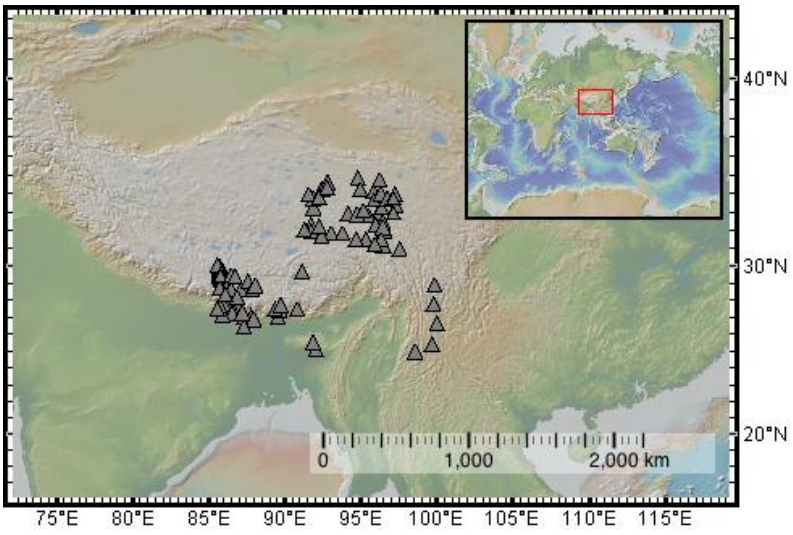

Figure 4.1: Map of all seismic stations used in the research including the temporary deployments.

Table 4.1: Stations network and coordinates. There are 211 stations in total.

Network	Station	Latitude	Longitude
X4	B02	32.9727	94.1388
X4	B02	32.9727	94.1388
YL	BIRA	26.484	87.267
XA	BUMT	27.5477	90.7664
YL	BUNG	27.8771	85.8909
X4	C08	34.2807	92.434
X4	C09	33.8612	92.2509
X4	C10	33.2576	91.8443
X4	C11	33.7864	91.8598
X4	C12	31.9859	91.7069
X4	C13	33.9965	91.5535
X4	C14	32.1019	91.2633
CB	CAD	31	97.5
XA	CHUK	27.0827	89.5503
X4	D01	34.1578	95.8316
X4	D06	33.7903	96.7344
X4	D07	34.7762	96.1667
X4	D08	34.9242	94.7805
X4	D10	34.3707	97.9234
X4	D11	34.0555	97.2094
X4	D12	33.4088	97.2767
X4	D13	33.0123	97.1132
X4	D14	32.9502	96.0821
X4	D15	32.8512	95.4374
X4	D16	33.2906	96.3635
X4	D17	33.7249	95.8419
X4	D18	32.8942	94.7009
X4	D19	34.2672	94.9184
X4	D21	31.8697	93.033
X4	D23	31.5421	95.2645
X4	D24	31.161	96.4715
X4	D25	31.9945	96.5117
X4	D26	32.4592	96.3942
YL	DINX	28.6646	87.1157
XA	DOCH	27.4922	89.6435
X4	F01	34.0535	96.3041
X4	F02	33.833	97.1024
X4	F03	32.8535	96.5826
X4	F04	32.3314	95.9731
X4	F05	32.2003	96.4311

X4	F06	33.1025	95.1146
X4	F12	31.514	96.3244
X4	F13	31.2393	95.9134
X4	F14	31.5572	94.6493
X4	F15	31.8747	93.7837
X4	F16	31.6949	92.4233
X4	F17	32.3861	91.7105
XF	H1000	29.2673	85.8577
XF	H1010	29.3355	85.8364
XF	H1020	29.413	85.7369
XF	H1030	29.483	85.7547
XF	H1040	29.5614	85.7398
XF	H1050	29.6387	85.7245
XF	H1060	29.7066	85.7082
XF	H1070	29.7767	85.7634
XF	H1071	29.7701	85.7749
XF	H1080	29.8502	85.7827
XF	H1090	29.9222	85.7329
XF	H1100	29.9936	85.6974
XF	H1110	30.0664	85.5526
YL	HILE	27.0482	87.3242
YL	ILAM	26.9102	87.9227
XI	JAFL	25.179	92.019
YL	JIRI	27.6342	86.2303
XO	JSO25	34.6429	92.8038
XO	JSO3	34.3751	92.7747
YL	LAZE	29.1403	87.5922
IC	LSA	29.7031	91.127
YL	MAZA	28.6713	87.8553
YA	MC06	28.9378	99.7942
YA	MC14	27.8646	99.7352
YA	MC15	26.7588	99.9883
YA	MC21	25.4876	99.6433
YL	MNBU	28.7558	86.161
YL	NAIL	28.6597	86.4126
CB	NAQ	32.25	92.25
XC	NB07	29.6517	94.7138
XF	NBIRA	26.484	87.267
XF	NBUNG	27.8771	85.8909
XF	NHILE	27.0482	87.3242
XF	NNAMC	27.8027	86.7146
XF	NPHAP	27.515	86.5842

XF	NRUMJ	27.3038	86.5482
XF	NSIND	27.2107	85.9088
XF	NSUKT	27.7057	85.7611
XF	NTHAK	27.5996	85.5566
XF	NTUML	27.3208	87.195
XA	PARO	27.5673	89.3205
XF	NPHAP	27.515	86.5842
YL	PHAP	27.515	86.5842
YL	PHID	27.1501	87.7645
YL	RBSH	28.1955	86.828
YL	RC14	29.4972	86.4373
YL	RUMJ	27.3038	86.5482
YL	SAJA	28.9093	88.0209
IN	SHL	25.5668	91.8559
YL	SIND	27.2107	85.9088
YL	SSAN	29.4238	86.729
XF	NSUKT	27.7057	85.7611
YL	SUKT	27.7057	85.7611
XA	TASH	27.7492	89.7309
XF	NTHAK	27.5996	85.5566
YL	THAK	27.5996	85.5566
CB	TNC	25.029	98.52
YL	TUML	27.3208	87.195
YL	XIXI	28.7409	85.6904
YL	YALA	28.4043	86.1133

4.2: RECEIVER FUNCTIONS METHOD

4.2.1: Introduction to Receiver Function:

The receiver function method is a relatively new technique to study the structure of Earth using the information from teleseismic earthquakes recorded at a three component seismograph. The has been continuously used and developed to characterize the detailed structure of crust and upper mantle and to obtain the information about the discontinuities in the crust and the upper mantle beneath the three component seismic stations. Recordings from earthquakes are often difficult to interpret due to reverberations near the source region and the extended waveforms generated by long-duration slip during an earthquake. This results in significant amount of overlap in the individual arrivals of waveforms (direct P wave, P to S conversions and other multiples within the crust). Receiver functions are generated by deconvolving the extended source pulses to improve the resolution of individual arrivals (Langston, 1979). The variation in travel time of the principle arrivals can be used to model the average P-wave and S-wave velocity structure beneath the stations.

4.2.2: Early Works in Receiver Functions:

The receiver function method was first introduced by Burdick and Langston (1977). They observed some energy in SV component of the receiver near the P wave arrival times and attributed it to the conversion of the direct P wave caused by the velocity discontinuity near the receiver. They used the forward modeling of waveforms to study the crustal velocity structures. An inversion technique was introduced by Ammon (1991), which helped the researchers to find

the velocity structures without previous knowledge of the local velocity discontinuities. Ammon (1991) used spectral deconvolution technique with water level of Clayton and Wiggins (1976).

Receiver functions are obtained by deconvolving the radial component from vertical, giving peaks indicating the positive and negative velocity contrast. Since the functions represent crustal and upper mantle structure below the receiver, they are named as receiver functions. Ligorria and Ammon (1999), developed a technique called "iterative time domain deconvolution" which is widely used today to estimate the receiver functions for the data with high signal to noise ratio.

While the first phase of the receiver functions is about obtaining the receiver functions for the stations, the second phase includes the estimation of the moho depth and the V_p to V_s ratio using the arrival times of the converted phases. Different techniques have been developed to convert the arrival times of converted phases to the depths including the joint inversion of receiver function with surface wave dispersion, the method of Zhu *et al.* (2006) and the method of Zhu and Kanamori (2000). The first method involving the surface wave dispersion requires large data and processing time and the method of Zhu et al. (2006) requires picking of the arrival times of the Ps phases by hand. The method of Zhu and Kanamori (2000) is equipped with automatic picking of the converted phases and requires less time for data processing.

4.2.3. Mathematical and Physical description of Receiver functions:

The receiver function method uses the fact that P waves beneath the seismic stations will generate a P to S converted phase at the velocity discontinuity below the receiver station (Shearer, 2009). This P to S converted phase is called a Ps phase, see Figure 4.2. In a 3

component broadband seismogram, the direct P energy mostly appears on the vertical component for the telesesimic events.

Unlike compressional (P) waves, shear waves (S) waves are characterized by having different polarization. In a typical case of S wave propagating in an isotropic medium, the polarized waves are called SV and SH which are the vertically and horizontally polarized S waves respectively. The SV wave is polarized in the plane of the propagation, whereas the SH wave is polarized orthogonal to it. If there is a layered medium, SV is polarized in the radial direction (source-receiver) and SH is polarized in the transverse direction. However, SH waves are not naturally generated by mode conversion at an interface like moho since they require transverse source excitation which require the relatively rare 9 component surveys with 3 component seismic sources and 3 component seismic sensors which generate and record the full elastic wavefield (Bale et al., 2009). To summarize, for the conversion of P to S phase at moho or other discontinuities beneath a 3 component receiver, we expect signal to be present on the horizontal radial component but not in the transverse component.

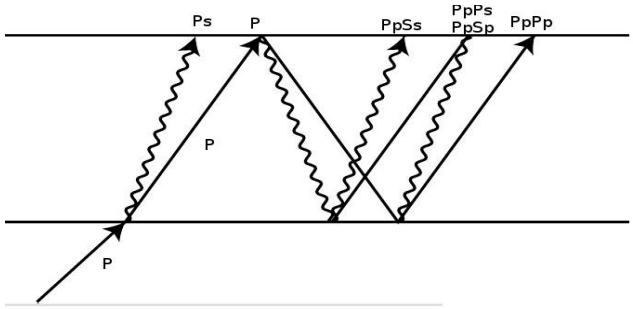

Figure 4.2: An upcoming P wave incident on a near-surface velocity discontinuity will generate a number of first-order converted and reflected phases. Modified after (Shearer, 2009)

In principle, we could estimate the depth of the discontinuity from the Ps-P time, but in practice Ps is hard to observe clearly in the individual seismograms as it is usually obscured by the coda of the P wave. So, it is necessary to extract the Ps signal from the direct P arrival which is done by first rotating the N and E horizontal components to the radial and transverse components and by deconvolving the radial component from the vertical.

There are two rotation systems commonly in practice. A ZRT rotation system is a 2 dimensional rotation where the Z component preserves the initial direction, see Figure 4.3, whereas, a LQT rotation is a 3 dimensional rotation with all the components of ZNE system being rotated. The two horizontal components N and E are rotated into the radial and transverse components in the following way.

$$\begin{bmatrix} R \\ T \\ Z \end{bmatrix} = \begin{bmatrix} \cos\theta & \sin\theta & 0 \\ -\sin\theta & \cos\theta & 0 \\ 0 & 0 & 1 \end{bmatrix} \begin{bmatrix} E \\ N \\ Z \end{bmatrix}$$

where $\theta = (3\pi/2-\Phi)$ and Φ is the back azimuth angle. The back azimuth describes the angle between the vector pointing from the seismic station to the source and the vector pointing from the seismic station to the north. The rotation is equivalent to the orthogonal transformation in 2 dimensions given by

$$A'=TA \qquad (4.1)$$

where A is the original ENZ system, A' is the new rotated system and T is the orthogonal matrix

$$T = \begin{bmatrix} \cos\theta & \sin\theta & 0 \\ -\sin\theta & \cos\theta & 0 \\ 0 & 0 & 1 \end{bmatrix}$$

The general transformation matrix for both ZRT and LQT system are given in (Upadhyay, 2004)

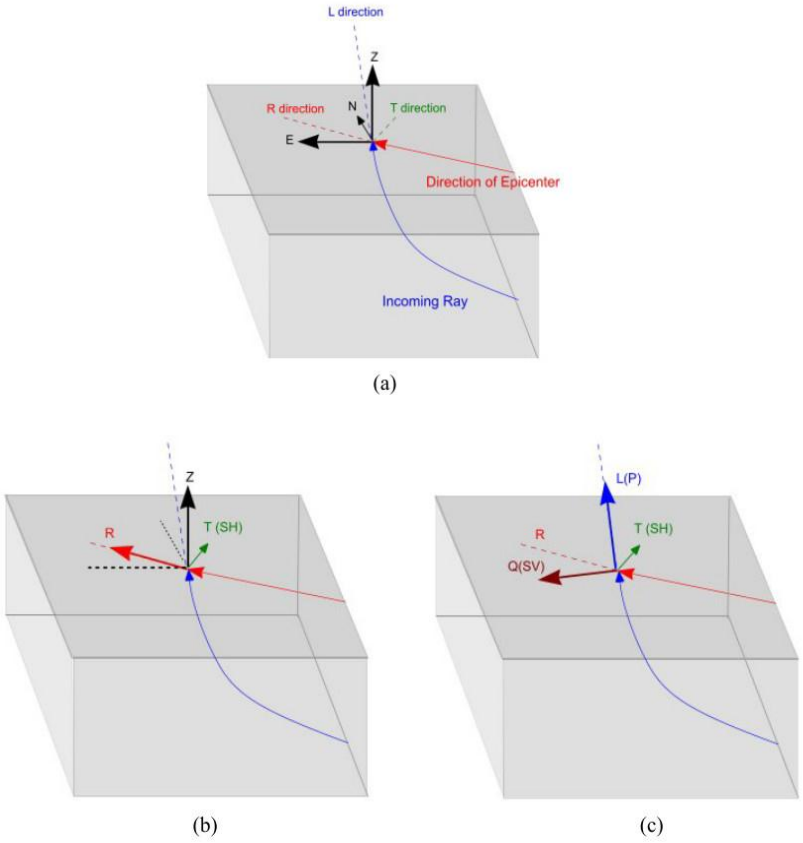

Figure 4.3: The rotation of coordinate systems for incoming events. (a) is the initial system of no rotation. (b) Rotation of the system to RTZ coordinate system, which is used in this study. (c) is the rotation of the system to QLT coordinate system which is similar to the RTZ system for teleseismic events.

A seismogram can be mathematically described as

$$S(t) = STF(t) * P(t) * I(t) \tag{4.2}$$

where S(t) is the seismogram, STF(t) is the source time function, P (t) is the along-path or propagation effect and I(t) is the instrument response.

Receiver functions are obtained by deconvolving the incoming vertical component from the radial component in order to remove the effects from source and propagation path, and therefore focus on the near surface structure. Let the original source time effect in frequency domain be S(ω), all the change which the signal goes through on its path be P(ω), the instrument response I(ω), and response to local velocity contrast near the receiver H(ω).

The signal in the vertical component is given by the Fourier transform of original time series signal as

$$Z(\omega) = S(\omega)\, P(\omega)\, I(\omega) \tag{4.3}$$

And the radial and transverse components of the signal are given as

$$R(\omega) = S(\omega)\, P(\omega)\, I(\omega)\, H\_R(\omega) \tag{4.4}$$

$$T(\omega) = S(\omega)\, P(\omega)\, I(\omega)\, H\_T(\omega) \tag{4.5}$$

where H_R(ω) and H_T(ω) are the near source effects for radial and transverse components in frequency domain.

So to find the receiver function, which represents the local velocity contrast we must divide radial component of the seismogram by the vertical component.

$$H\_R\ (\omega) = \frac{R(w)}{Z(w)} \tag{4.6}$$

And similarly for the transverse component

$$H\_T\ (\omega) = \frac{T(w)}{Z(w)} \tag{4.7}$$

These divisions in the frequency domain correspond to the deconvolution in time domain. The inverse Fourier transforms of the H_R(ω) and H_T(ω), H_R(t) and H_T(t) respectively, are called the radial and transverse receiver functions and indicate the velocity contrast near the receiver.

Since the deconvolution can be done either in frequency domain or in time domain, we have deconvolution techniques for both the domains. Two general methods of deconvoltion are described below.

4.2.4: Receiver Function Estimation

4.2.4.1: Frequency domain deconvoltion with water level:

Frequency domain deconvolution technique is the direct solution to the equation (4.4).

For this, the radial and horizontal components of the seismograms are transformed into frequency domain using Fourier Transform. The result of division of them yields the receiver function.

Let w represent angular frequency (2*pi*f), Z(w) and R(w) represent the Fourier transforms of the vertical, radial components of motion, and E_R(w) the Fourier transform of the radial receiver function. The receiver function is defined by

$$E\_R(w) = R(w)\, Z^*(w) / Z(w)Z^*(w) \tag{4.8}$$

While the above equation is the definition of a receiver function, it cannot be used to compute observed seismograms because small or zero values of Z(w)Z*(w) cause numerical problems in the calculation. A simple solution to the problem is an approach called water-level deconvolution. This was the approach adopted by Langston (Langston, 1979) and is still a very good method when the data quality is good. In water-level deconvolution, the way we avoid division by small numbers is to replace small values in the denominator with a fraction of the maximum value (for all frequencies) of the denominator. The fraction is called the water-level parameter (the water-level is the fraction multiplied by the maximum denominator amplitude), and is chosen by trial and error.

The advantages of this technique are that it is fast and relatively simple. The drawback is that it might give false bumps in receiver function which are not a result of a velocity contrast in seismograms of stations in which the signal to noise ratio is high.

4.2.4.2: Iterative time-domain deconvolution:

Iterative time domain deconvolution technique (Ligorría and Ammon, 1999) relies on the cross-correlation function, which measures the similarity of two waveforms as a function of a time-lag applied to one of them. It is the integral of the product of two signals, one of which is shifted in the time domain. It is related to convolution except the shifted signal is not also flipped (Bracewell, 1986). Cross correlation in the time domain is equivalent to multiplication with a conjugate complex in the frequency domain.

In receiver-function estimation, iterative deconvolution method uses least-squares minimization of the difference between the Gaussian filtered observed horizontal seismogram and a predicted signal generated by the convolution of an iteratively updated spike train with the vertical-component seismogram. First, the vertical component is cross-correlated with the radial component to estimate the lag of the first and largest spike in the receiver function. The spike amplitude is estimated by solving a simple equation given by Kikuchi and Kanamori (Kikuchi and Kanamori, 1982). Then the convolution of the current estimate of the receiver function with the vertical-component seismogram is subtracted from the radial-component seismogram, and the procedure is repeated to estimate other spike lags and amplitudes. Mathematically, the algorithm is given as

$$R(t) - E\_R_i(t) * Z(t) \tag{4.9}$$

where $E\_R_i(t)$ is the i^{th} iteration of the receiver function, R(t) and Z(t) are the radial(horizontal) and vertical signals respectively.

The difference gives the misfit between the vertical and receiver-function convolution and the radial component seismogram, which is reduced with each additional spike in the receiver function, and the iteration stops when the reduction in misfit with additional spikes becomes insignificant. The radial receiver functions are computed using a Gaussian width factor which controls the bandwidth of the signal. The larger the value of Gaussian factor, larger is the bandwidth. The Gaussian factor of 2.5 is generally used in the receiver function analysis (Ligorría and Ammon, 1999).

There are several advantages of iterative time domain deconvolution technique over the other methods. Some advantages of this technique (Kosarian, 2006) are given below. The iterative deconvolution method is constructed as a sum of Gaussian pulses which produces a flat spectrum at the longest period, a feature common to all simple earth models. The flat long period spectrum can be considered as a priori information that helps to reduce side-lobes caused by the spectral or singular value truncation stabilization procedure. The reduction in the side-lobes can help ease the interpretation. The iterative deconvolution requires no choice of an optimal stabilization parameter such as water level or damping value.

Deconvolution technique usually includes a Gaussian low pass filter which reduces the amplitude of short period fluctuations dominated by scattering effects. This simple shape of Gaussian is chosen after (Langston, 1977) and (Owens et al., 1984). The filter G(ω) is defined in the frequency domain by

$$G(\omega) = exp(-w^2/4\,a^2) \tag{4.10}$$

where a is known as the Gaussian width parameter and w is the angular frequency($2\pi f$).

4.2.5 H-K Stacking:

The depth of the Moho discontinuity can be calculated after identifying the peak which represents Moho conversion in the receiver function waveform. The receiver function only gives the delay time between P wave and converted S wave. Converting the delay time to depth requires some knowledge of the Vp/Vs ratio which is referenced as K. If such knowledge is not present, the arrival times of the reverberated phases, also known as multiples, can be used to constrain K and H. The average crustal thickness, H, and Vp/Vs ratio beneath a seismic station is estimated from principal conversion phase Ps and their first-order reverberations PpPms and (PpSms + PsPms) in the RF time-series using H-k stack method(Zhu and Kanamori, 2000).

The first-order information about the crustal structure under a station can be derived from the radial receiver function which is dominated by P-to-S converted energy from a series of velocity discontinuities in the crust and upper mantle. The moho is usually represented by the largest signal after the first P arrival due to the large velocity contrast at the crust mantle boundary. The difference in arrival time between this conversion Ps and P can be used to find the crustal thickness, given the average crustal velocities (Zhu and Kanamori, 2000). The crustal thickness can be calculated using the relation

$$H = \frac{tPs}{\sqrt{\frac{1}{Vs^2} - p^2} - \sqrt{\frac{1}{Vp^2} - p^2}} \tag{4.11}$$

where p is the ray parameter, of the incident wave tPs is differential travel time of S wave with respect to P wave in the crust and Vs and Vp are the average P and S wave crustal velocities.

From equation (4.9) it is clear that the dependence of H on Vp is not as strong as in Vs(or Vp/Vs) since crustal thickness is proportional to the difference in arrival time of P and S waves. The dependence of H on Vp/Vs (K) is given by

$$\Delta H = \frac{\partial H}{\partial K}\Delta K \tag{4.12}$$

This ambiguity is reduced by later arriving phases which provide additional constraints on H so that both H and K can be estimated(Zhu and Kanamori, 2000)

$$H = \frac{tPpPs}{\sqrt{\frac{1}{Vs^2}-p^2}+\sqrt{\frac{1}{Vp^2}-p^2}} \tag{4.13}$$

$$H = \frac{tPpPs+PsPs}{\sqrt{\frac{1}{Vs^2}-p^2}} \tag{4.14}$$

In real situation, it is very difficult to identify the moho Ps and the multiples by measuring the their arrival times on a single receiver function due to background noise, scattering from crustal heterogeneties and conversion from other velocity discontinuities. To increase the signal to noise ratio (SNR), one can use multiple events to stack their receiver functions which are done in number of time domain events. The time domain receiver functions are stacked to the H-K domain in order to find the crustal thickness and the Vp/Vs ratio in the following way (Zhu and Kanamori, 2000)

$$s(H,K) = w_1 r(t_1) + w_2 r(t_2) - w_3 r(t_3) \quad (4.15)$$

where r(t) is the radial receiver function t_1, t_2 and t_3 are he predicted arrival time for Ps, PpPs, and PpSs+PsPs phases respectively corresponding to crustal thickness H and Vp/Vs K. The w_i's are the weight factors and sum to 1. The stacked function *s*(H,K) when all three phases are stacked coherently

Although there are other methods to solve the depth problem including the inversion techniques, this method by Zhu and Kanamori has some salient features. Some advantages of this method include: convenient processing of large amount of teleseismic waveforms, no need of picking arrival times for different phases and estimation of uncertainties from flatness of *s*(H,K) at the maximum.(Zhu and Kanamori, 2000)

4.3: PROCESSING

In this study, we used waveforms from the earthquakes epicentral distance between 30 and 90 degrees. The epicentral distance less than 30 degrees are affected by the interaction of P waves with the transition zone and epicentral distance greater than 90 degrees can complicate the response due to interaction with core. Events with magnitude greater than 5.9 are used in order to have a good signal to noise ratio in our data. The continuous 3 component seismograms are first processed to remove the mean and trend and tapered with a Hanning window of width 0.1 to include the useful frequencies for a teleseismic event. The back azimuth angles are obtained with the locations of the stations and the epicenter for each events and two horizontal components are rotated to the radial and transverse components by varying the back azimuth by $\pm 5, \pm 10$and ± 15degrees. Then the vertical component is deconvolved from the radial

component using an iterative, time-domain deconvolution algorithm following Ligorría and Ammon (1999). All receiver functions are processed using Gaussian width parameters of 1.00, 1.75 and 2.50. The deconvolution consisted of large number of iterations and the receiver functions for which the percentage fit to equation (3.7) < 80% are rejected and are considered as bad data. The resulting source equalized time series are P wave receiver functions. Figure 3.4 shows a three component seismogram for station ILAM and the corresponding receiver functions.

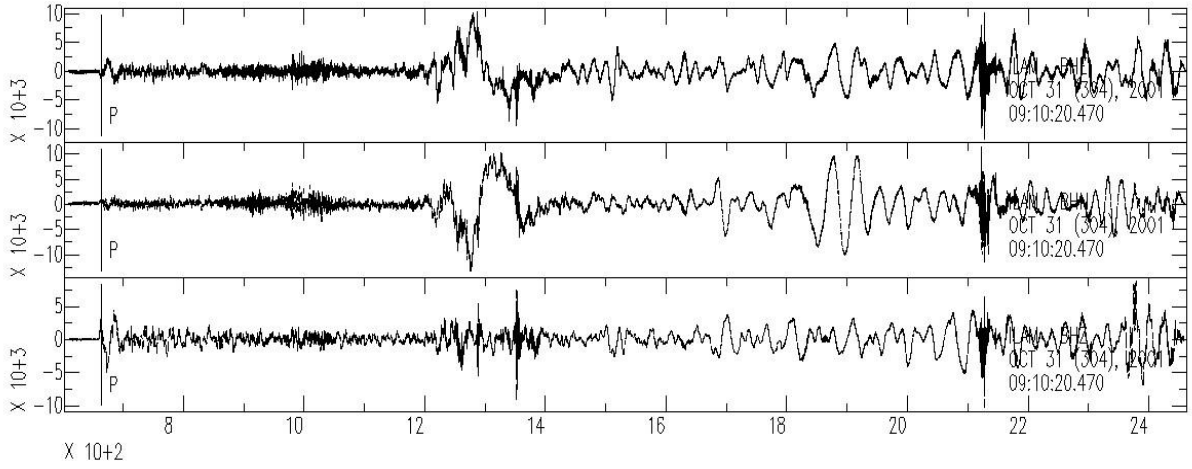

(a)

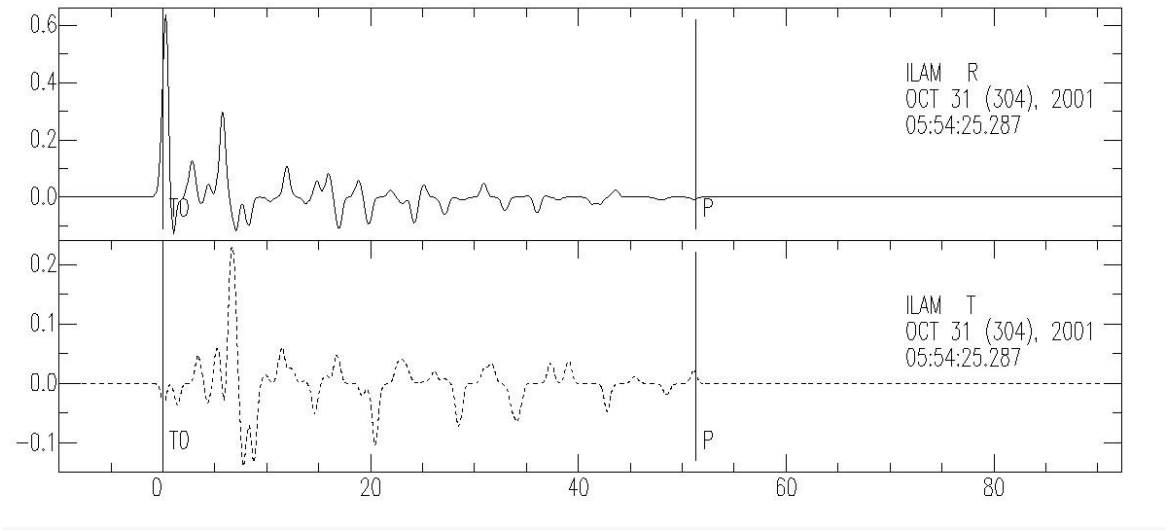

(b)

Figure 4.4: (a) A three component waveform, top, E-W, middle N-S and bottom, Z(vertical) for 2001/10/31 earthquake recorded at station ILAM in eastern Nepal. (b) Corresponding radial(top) and transverse(bottom) receiver functions.

Raw receiver functions chosen for further analysis are selected based on the following criteria. First, amplitude at time, t=0 should be positive and the maximal spike should be at t=0 to ensure the direct P arrival always appears at time zero. Secondly, it is made sure that the root mean square (RMS) misfit of the amplitude against the back azimuth are minimum for the transverse receiver function and the radial and transverse receiver functions set with minimum RMS value for the transverse component are selected for further processing. Since theoretically, there should be no energy in the transverse component which consist of the horizontally polarized SH phases, we only include the radial receiver functions for which the corresponding transverse receiver function has the minimum amplitude. However, non-zero amplitudes are seen

in the transverse component which can be attributed to presence of dipping and perhaps non polar velocity contrast or anisotropy (Langston, 1977).

Finally, only the receiver functions having a clear P and Ps arrival phases and smaller amplitude for the other reverberations are considered as good receiver functions and all other receiver functions are handpicked and discarded. As a result, 3246 qualified radial receiver functions are manually selected out of total 8171 radial receiver functions. Figure 3.6 shows examples of good and bad receiver function for station ILAM.

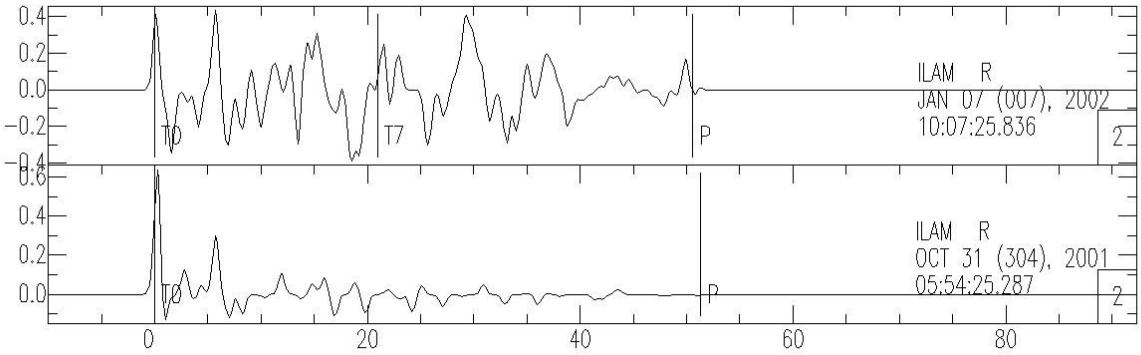

Figure 4.5: Examples of receiver functions for station ILAM, top, discarded receiver function and bottom, a good receiver function. T7 marking is used in SAC to select all the bad receiver functions and sort as poor data.

In order to make an estimate of the crustal thickness and Poisson's ratio with the assumption of an average P-wave velocity of the crust, it is necessary to find the ray parameter and travel time for the P arrival which is done using the taup_time package in the TauP toolkit

(Crotwell et al., 1999) developed by the seismologists at the University of South Carolina. The ray parameter (p) characterizes a wave's ray path via its slowness (reciprocal of the apparent velocity) and is constant for a ray path for different wave phenomena like reflection, refraction and transmission at a certain velocity contrast

Chapter 5: Results and Discussion

5.1: Crustal Thickness and V_P/V_S ratio measurements

The crustal thickness and V_P/V_S ratio measurements were performed for 99 stations out of total 211 stations for which the data was obtained. The H-K stacking method of Zhu and Kanamori(Zhu and Kanamori, 2000) was used to convert the time domain receiver functions into H-K domain and obtain the values of crustal thickness and the ratio of the P and S wave velocities. For all the stations, the pmS conversion from the moho are identified on stacked receiver functions. As mentioned in the processing section only the radial receiver functions corresponding to minimum amplitude in the transverse receiver functions were selected for further processing (see Figure 5.1).

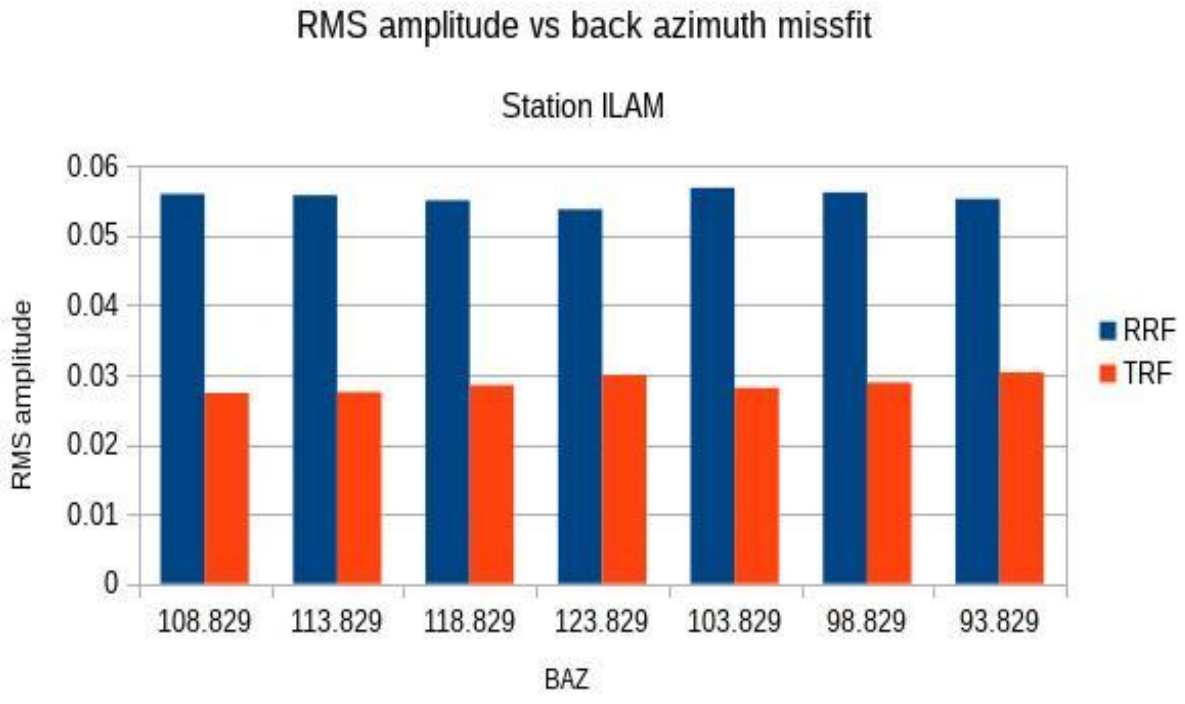

Figure 5.1: RMS amplitude vs. Back Azimuth (BAZ) angle for the radial and transverse receiver functions estimated for station ILAM for 2001/10/31 event. Transverse receiver function with BAZ angle 108.829° has the minimum RMS amplitude and hence the corresponding radial receiver function is selected for further processing.

The main trend in the receiver function analysis across the Himalaya from our study reflects the deepening of the moho from about 40 km beneath southern Nepal to about 80 km in southern Tibet. A locally steeper moho deep is obtained in the high range of Himalayas. The results for four of the main geological divisions are presented in this section. The results for all the stations are shown in Table 5.1

Station: **SIND**

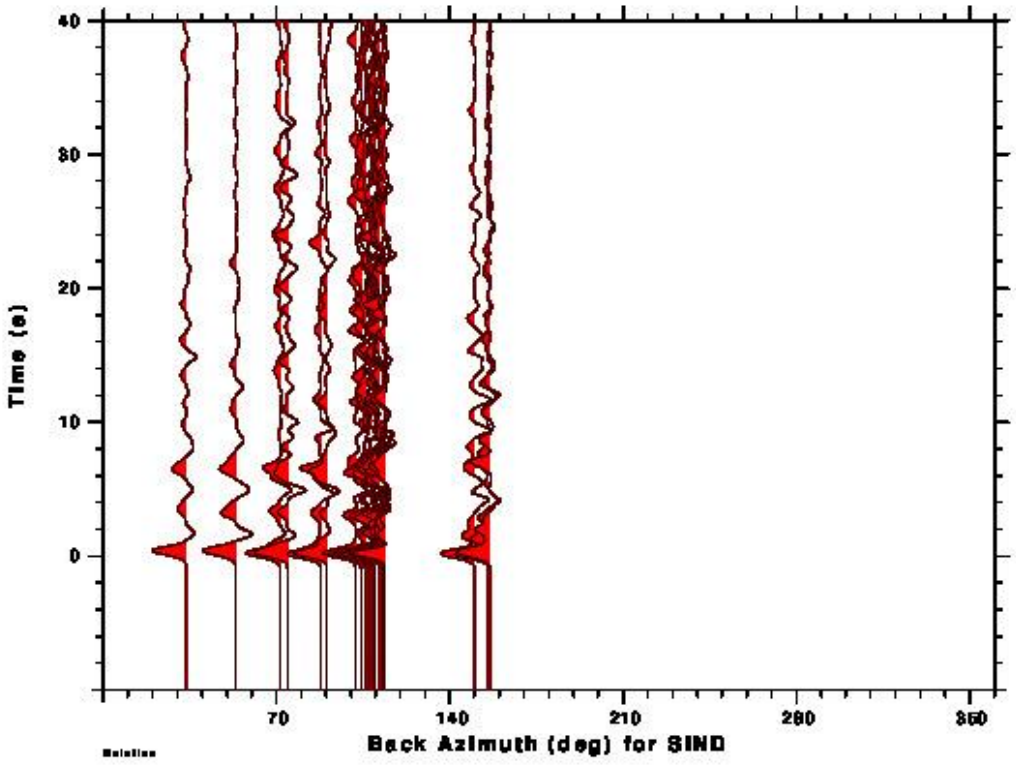

Figure 5.2: Radial receiver functions for station SIND plotted as a function of back azimuth.

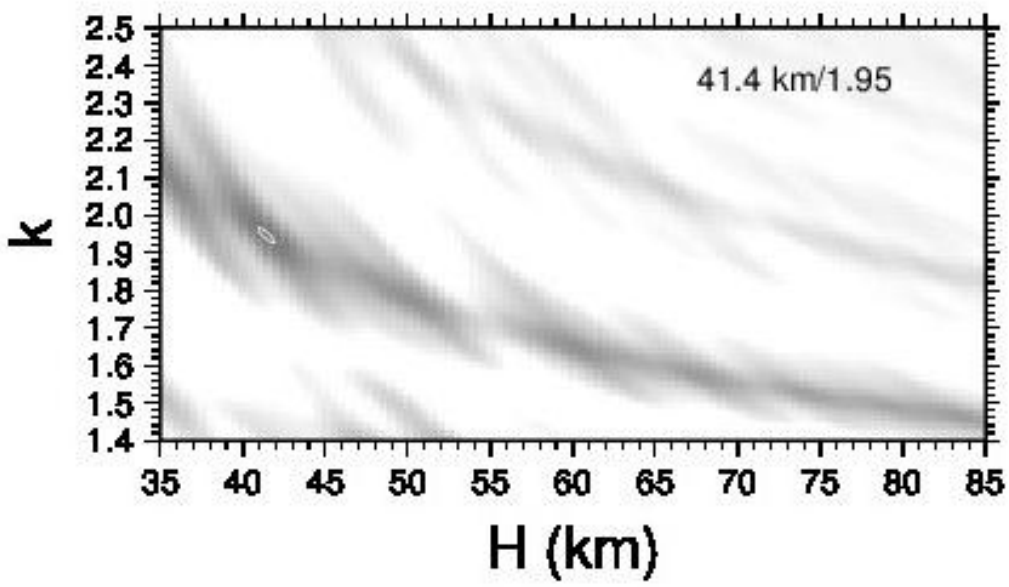

Figure 5.3: Vp/Vs ratio versus crustal thickness for the station SIND calculated using the receiver function stacking technique of Zhu & Kanamori.

There were a total of 22 receiver functions for station SIND which were stacked to obtain the H vs. K plot. Figure 4.2 shows all the receiver functions plotted against back azimuth. A phase can be noticed (Figure 5.2) at ~6 seconds which probably represents primary moho conversion. This is followed by week positive arrivals at later time which represents the reverberated phases.

The moho depth and V_P/V_S ratio for SIND were found to be 41.4 ± 0.33 km and 1.95 ± 0.09 respectively.

Station SIND was a temporary deployment as a part of HIMNT experiment and was located in Sindhuli District, southeast of Kathmandu at an elevation of 465 meters. The station collected data for 2 years between 2001 and 2003.

Station: **PHAP**

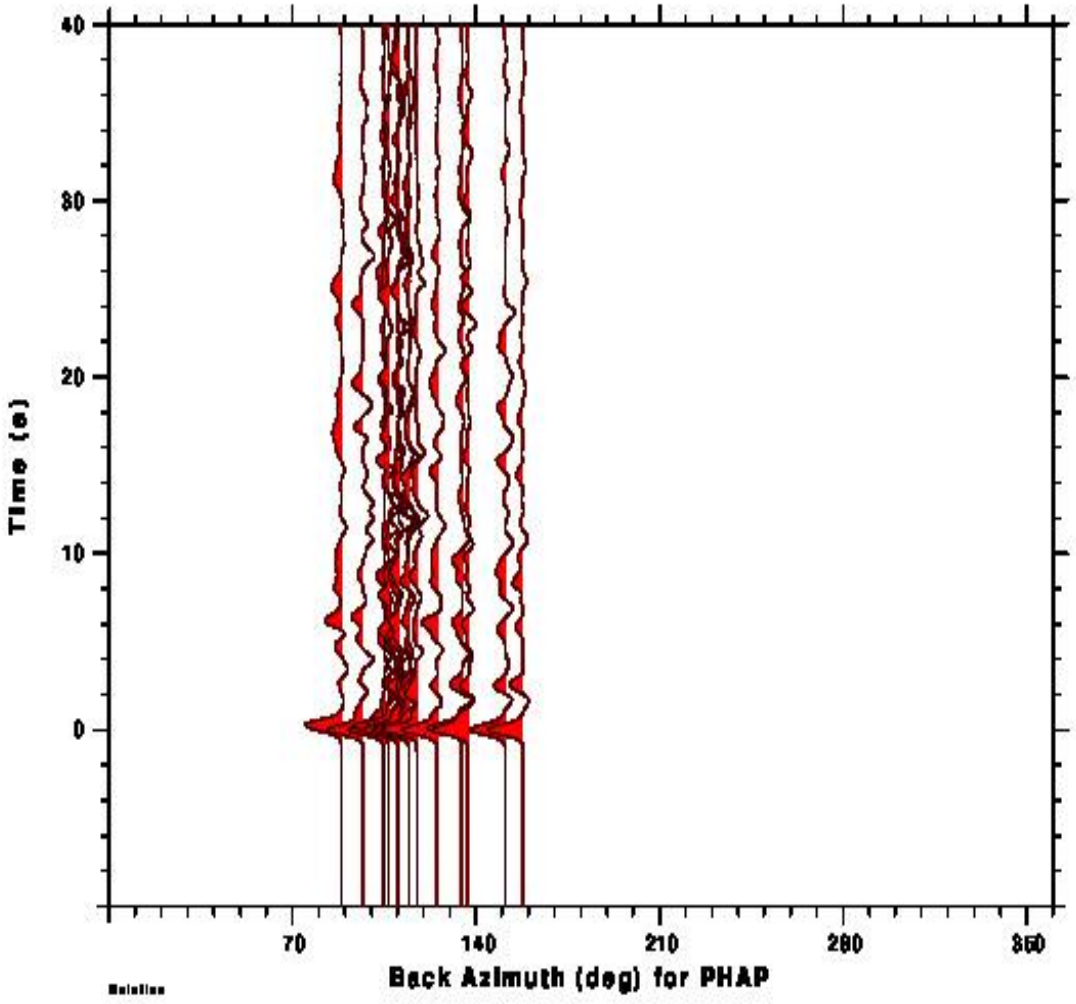

Figure 5.4: Radial receiver functions for station PHAP plotted as a function of back azimuth.

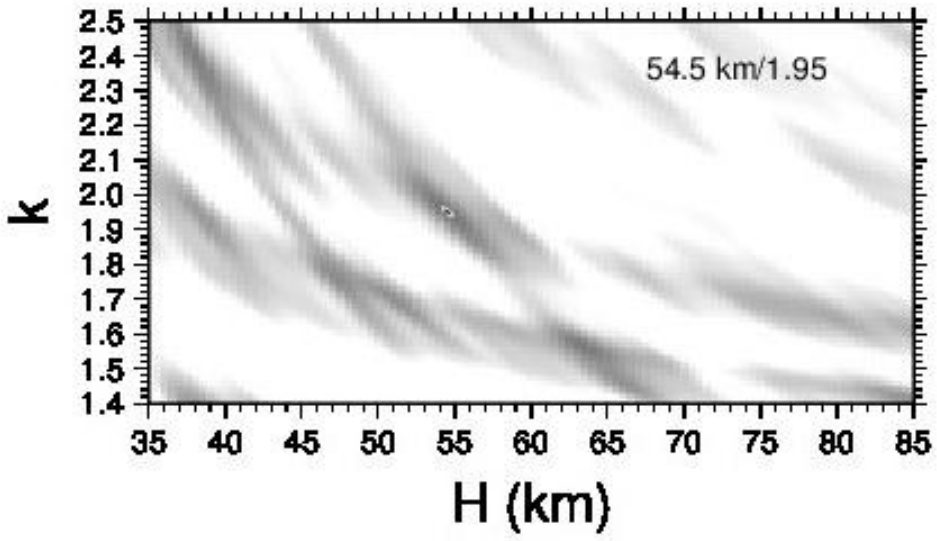

Figure 5.5: Vp/Vs ratio versus crustal thickness for the station PHAP calculated using the receiver function stacking technique of Zhu & Kanamori.

A total of 16 receiver functions were obtained for the station PHAP northeast of Kathmandu at an elevation of 2488 meters. The moho depth and the V_P/V_S ratios for station PHAP were found to be 54.5 ± 0.21 km and 1.95 ± 0.07respectively. Station PHAP lies in Salleri District in Nepal and is geologically situated in the Lesser Himalayas above the Siwalik Range.

Station: **MC15**

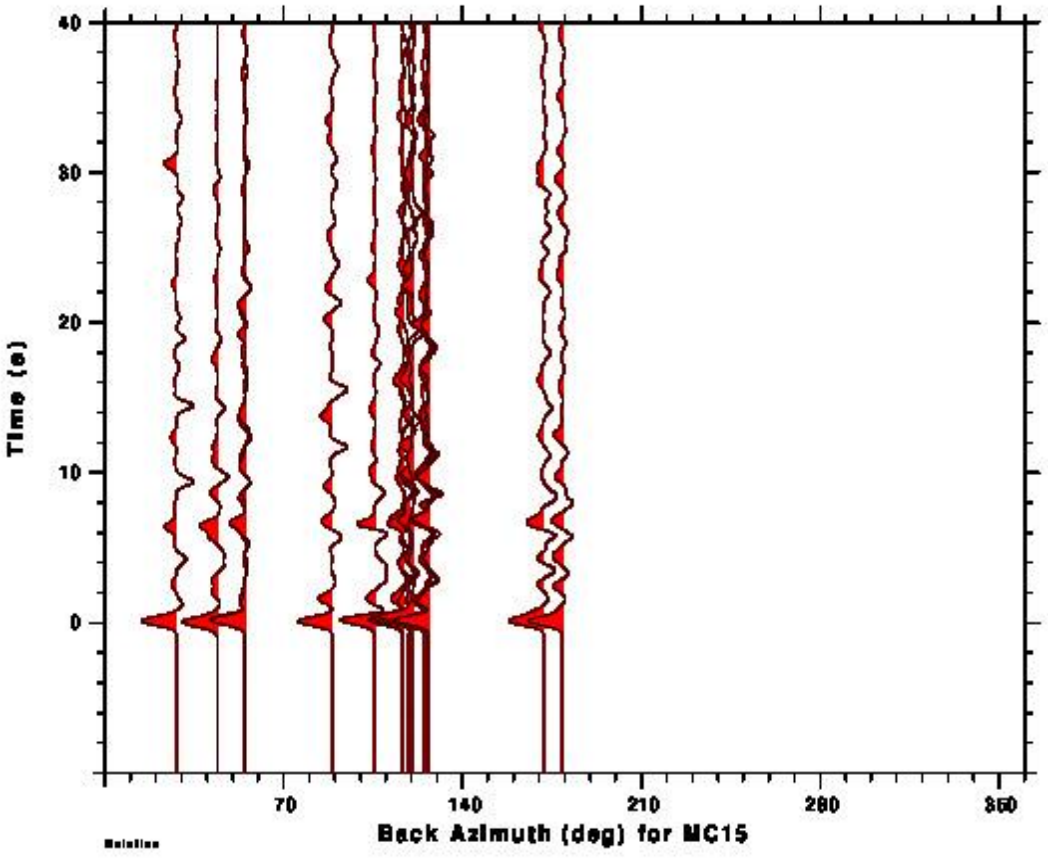

Figure 5.6: Radial receiver functions for station MC15 plotted as a function of back azimuth. The station MC15 (26.75 ˚N and 99.98 ˚E) lies in the eastern region of this study and the results for this station along with the adjoining stations help to understand the lateral variation of moho depth.

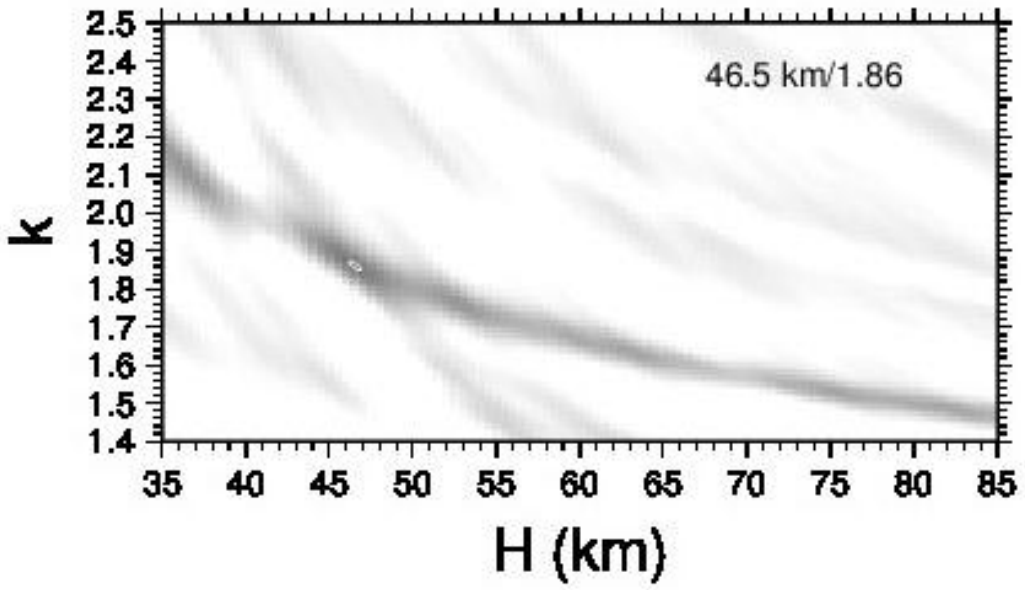

Figure 5.7: Vp/Vs ratio versus crustal thickness for the station MC15 calculated using the receiver function stacking technique of Zhu & Kanamori

Station MC15 represents the east most region in our study and lies above Yunnan region in South China. Figure 4.6 shows clear arrival of Ps phase for this station little after 6 seconds after the first P arrival. The moho depth and the V_P/V_S ratio for station MC15 were found to be 46.54 ± 0.22 km and 1.86 ± 0.07 respectively. The values of moho depth and V_P/V_S ratio are in the range of the values obtained in the western regions of our study in Nepal.

Station: **H1030**

Station H1030 was a part of Hi-CLIMB experiment which collected data for one year in 2004-2005 and lies in the Higher Himalayan range of the Nepal-Tibet Himalayan orogen.

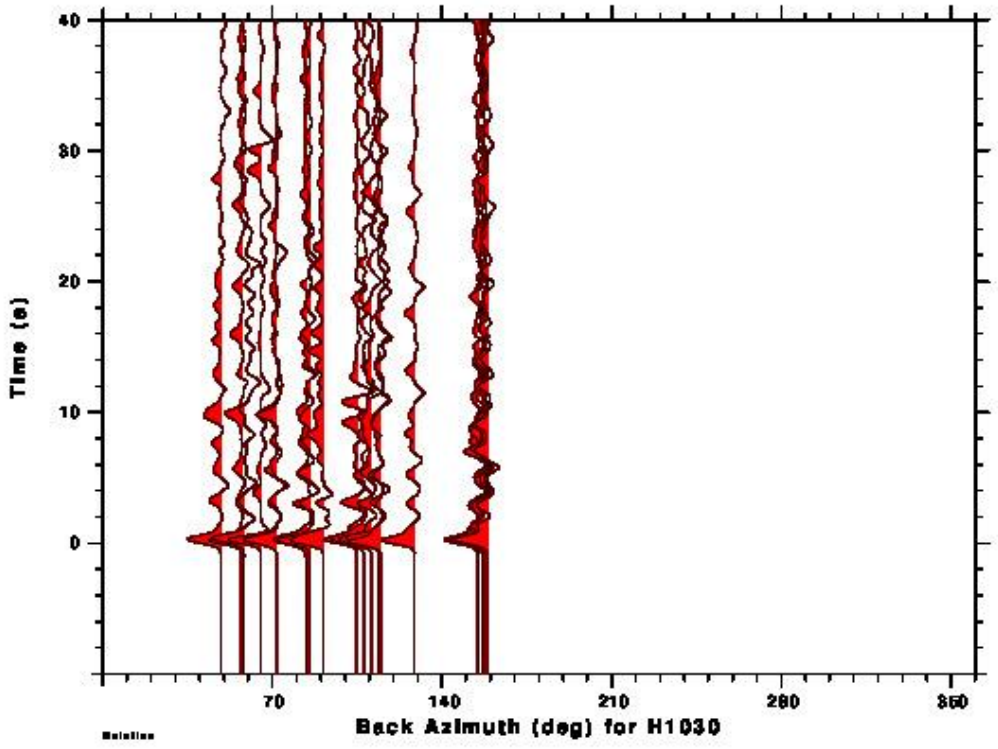

Figure 5.8: Radial receiver functions for station H1030 plotted as a function of back azimuth.

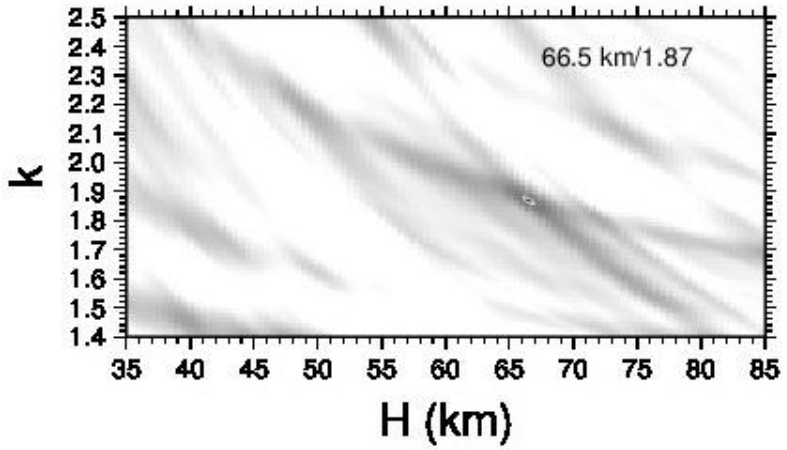

Figure 5.9: Vp/Vs ratio versus crustal thickness for the station H1030 calculated using the receiver function stacking technique of Zhu & Kanamori

There is a clear arrival of Ps phase for the H1030 station at ~10 seconds after the first P arrival. The arrival time after the first P arrival has increased significantly as we expected and a higher moho depth is obtained. The moho depth and the V_P/V_S ratio for station H1030 were found to be 66.50 $\pm$ 0.25 km and 1.87 $\pm$ 0.07 respectively.

Station: **B02**

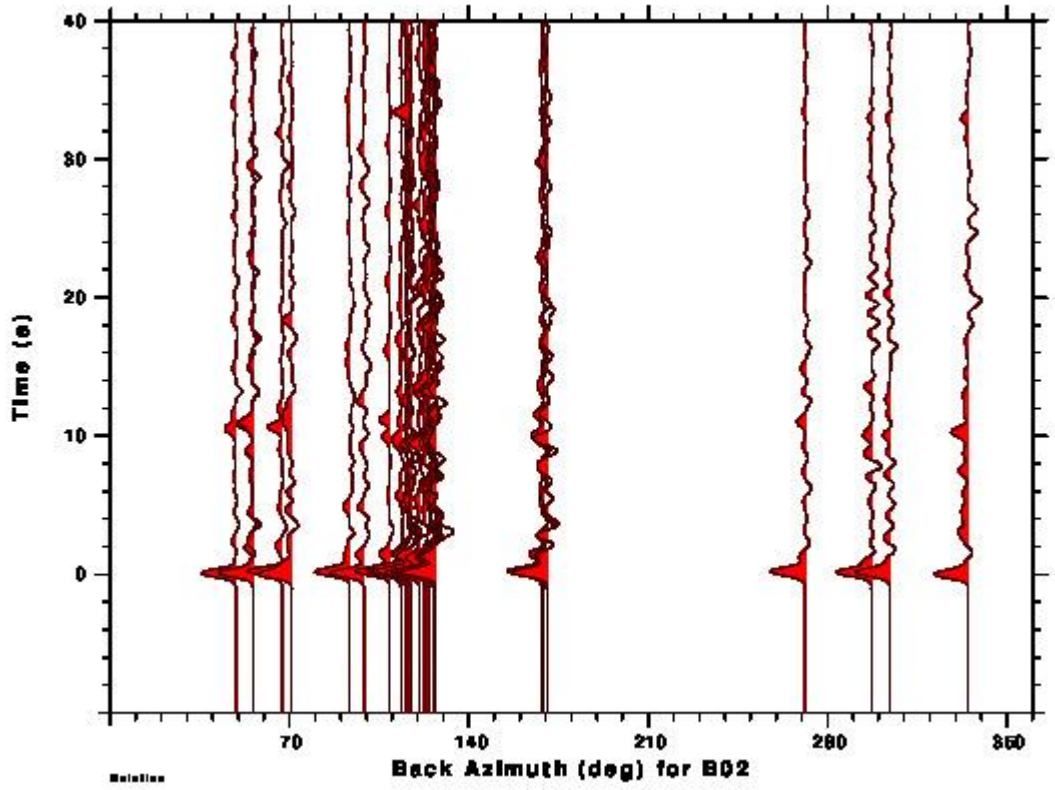

Figure 5.10: Radial receiver functions for station B02 plotted as a function of back azimuth

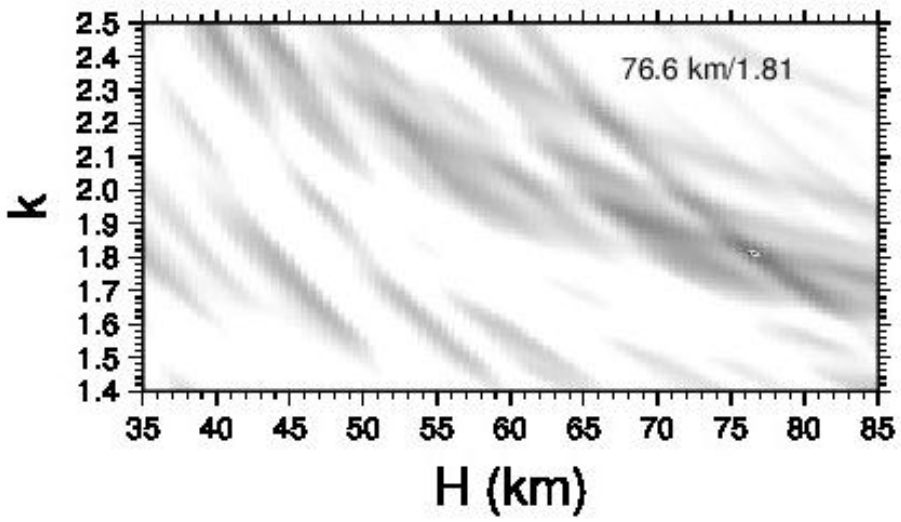

Figure 5.11: Vp/Vs ratio versus crustal thickness for the station B02 calculated using the receiver function stacking technique of Zhu & Kanamori (2000).

Station B02 (32.97 ˚N, 94.13 ˚E) lies above the Higher Himalayas in the Tethyan region of the Himalayan arc. The first significant conversion is ~11 seconds after the first P arrival which represents the conversion at moho in that region. Although not all the receiver functions show a clear conversion, results from few receiver functions are good enough to interpret the arrival as the Ps phase. A total of 29 receiver functions were obtained and stacked together for station BIRA. The moho depth and the V_P/V_S ratio for station H1030 were found to be 66.50 ± 0.25 km and 1.87 ± 0.07 respectively. Station D14 at about same latitude as that of B02 but further east had the value of 81 for the moho depth, the highest value in our results.

Although all the stations do not have the value of moho depth and V_P/V_S as expected, in overall, the results were consistent with the general trend of increasing moho depth from southern plains to the Tibetan Himalayan range. Table 5.1 shows the results for moho depth and V_P/V_S ratio for all the stations with the error.

Table 5.1: Results for all the stations

Station	Latitude (°N)	Longitude (°E)	Moho depth(H) (km)	Δ H (km)	V_P/V_S(K)	Δ K	No.of RF_S
B02	32.9727	94.1388	76.61	0.17	1.81	0.05	29
BIRA	26.484	87.267	42.01	0.15	1.56	0.05	3
BUMT	27.5477	90.7664	36.00	0.01	1.40	0.01	14
BUNG	27.8771	85.8909	36.49	0.25	1.83	0.08	16
C08	34.2807	92.434	35.00	0.01	2.43	0.00	48
C09	33.8612	92.2509	67.08	0.29	1.81	0.07	104
C10	33.2576	91.8443	63.54	0.26	1.82	0.07	104
C11	33.7864	91.8598	59.10	0.29	1.87	0.08	119
C12	31.9859	91.7069	72.53	0.24	1.72	0.07	84
C13	33.9965	91.5535	43.43	0.67	1.61	0.08	54
C14	32.1019	91.2633	40.52	0.31	2.34	0.08	10
CAD	31	97.5	73.58	0.31	1.71	0.06	106
CHUK	27.0827	89.5503	48.43	0.20	1.75	0.06	13
D01	34.1578	95.8316	38.97	0.25	2.40	0.06	72
D06	33.7903	96.7344	58.37	0.30	1.95	0.07	66
D07	34.7762	96.1667	65.49	0.61	1.78	0.09	46
D08	34.9242	94.7805	68.51	0.40	1.70	0.10	48
D11	34.0555	97.2094	62.08	0.25	1.81	0.07	10
D12	33.4088	97.2767	55.99	0.18	1.78	0.06	212
D13	33.0123	97.1132	70.65	0.22	1.79	0.07	62
D14	32.9502	96.0821	81.16	0.34	1.59	0.06	29
D15	32.8512	95.4374	37.94	0.25	2.03	0.07	73
D16	33.2906	96.3635	75.37	0.21	1.72	0.06	14
D17	33.7249	95.8419	46.03	0.22	1.54	0.07	78
D18	32.8942	94.7009	73.49	0.21	1.70	0.06	52
D19	34.2672	94.9184	65.89	0.44	1.84	0.07	42
D21	31.8697	93.033	39.01	0.18	2.42	0.06	28
D23	31.5421	95.2645	39.45	0.19	2.44	0.07	40
D24	31.161	96.4715	38.48	0.30	2.47	0.08	33
D25	31.9945	96.5117	35.00	0.01	1.41	0.00	30
D26	32.4592	96.3942	35.50	0.23	1.48	0.07	24
DINX	28.6646	87.1157	79.55	0.16	2.48	0.04	3
DOCH	27.4922	89.6435	36.51	0.22	2.09	0.07	10
F01	34.0535	96.3041	48.89	0.21	2.05	0.07	58
F02	33.833	97.1024	35.98	0.22	1.42	0.07	55
F04	32.3314	95.9731	59.53	0.43	2.08	0.07	42
F05	32.2003	96.4311	36.53	0.21	1.83	0.07	49
F06	33.1025	95.1146	39.52	0.35	2.00	0.09	36
F12	31.514	96.3244	52.54	0.22	1.98	0.07	9
F13	31.2393	95.9134	43.03	0.24	2.28	0.07	26
F14	31.5572	94.6493	71.83	0.26	1.67	0.06	71
F15	31.8747	93.7837	75.50	0.21	1.68	0.06	22
F16	31.6949	92.4233	78.41	0.39	1.68	0.06	38
F17	32.3861	91.7105	60.05	0.23	1.86	0.08	58
H1000	29.2673	85.8577	54.06	0.22	2.08	0.08	8
H1010	29.3355	85.8364	50.48	0.27	2.14	0.08	19

H1020	29.413	85.7369	63.51	0.71	1.87	0.07	23
H1030	29.483	85.7547	66.50	0.25	1.87	0.07	20
H1040	29.5614	85.7398	56.93	0.42	1.99	0.08	20
H1050	29.6387	85.7245	57.43	0.44	1.97	0.07	24
H1060	29.7066	85.7082	55.42	0.22	1.97	0.07	22
H1070	29.7767	85.7634	57.09	0.92	1.99	0.07	7
H1071	29.7701	85.7749	50.46	0.18	2.46	0.07	8
H1080	29.8502	85.7827	62.47	0.20	1.94	0.06	12
H1090	29.9222	85.7329	37.96	0.41	2.40	0.07	24
H1100	29.9936	85.6974	69.54	0.27	1.65	0.06	30
H1110	30.0664	85.5526	39.44	0.27	1.56	0.09	33
HILE	27.0482	87.3242	35.00	0.00	1.40	0.00	42
ILAM	26.9102	87.9227	35.46	0.34	1.95	0.09	10
JAFL	25.179	92.019	83.66	0.23	1.50	0.06	45
JIRI	27.6342	86.2303	50.50	0.26	1.76	0.07	5
JSO25	34.6429	92.8038	58.00	0.50	1.97	0.09	74
JSO3	34.3751	92.7747	71.10	0.27	1.49	0.06	20
LAZE	29.1403	87.5922	35.00	0.02	1.45	0.01	11
LSA	29.7031	91.127	37.87	0.24	1.42	0.08	103
MAZA	28.6713	87.8553	58.97	0.18	1.56	0.05	9
MC06	28.9378	99.7942	66.09	0.24	1.57	0.06	13
MC14	27.8646	99.7352	35.47	0.19	1.70	0.06	25
MC15	26.7588	99.9883	46.54	0.22	1.86	0.07	16
MC21	25.4876	99.6433	47.40	0.25	1.70	0.07	15
MNBU	28.7558	86.161	56.98	0.19	1.80	0.06	14
NAIL	28.6597	86.4126	50.97	0.25	1.91	0.07	9
NAQ	32.25	92.25	66.58	0.33	1.83	0.08	82
NBIRA	26.484	87.267	37.53	0.18	1.57	0.06	3
NBUNG	27.8771	85.8909	50.99	0.32	1.61	0.08	5
NHILE	27.0482	87.3242	38.88	0.21	1.63	0.07	10
NPHAP	27.515	86.5842	71.00	0.25	2.08	0.05	3
NRUMJ	27.3038	86.5482	42.63	0.17	1.86	0.07	4
NSIND	27.2107	85.9088	41.48	0.22	1.96	0.07	6
NSUKT	27.7057	85.7611	38.50	0.21	1.45	0.06	3
NTHAK	27.5996	85.5566	35.00	0.01	1.43	0.01	2
NTUML	27.3208	87.195	57.43	0.20	1.51	0.06	3
PARO	27.5673	89.3205	49.55	0.22	1.42	0.06	32
PHAP	27.515	86.5842	54.53	0.21	1.95	0.07	16
PHID	27.1501	87.7645	45.97	0.22	1.55	0.06	11
RBSH	28.1955	86.828	35.00	0.01	1.73	0.01	12
RC14	29.4972	86.4373	44.99	0.18	1.42	0.06	17
RUMJ	27.3038	86.5482	42.09	0.30	1.83	0.09	18
SAJA	28.9093	88.0209	52.43	0.30	1.92	0.08	7
SHL	25.5668	91.8559	35.00	0.01	1.66	0.01	12
SIND	27.2107	85.9088	41.42	0.33	1.95	0.09	22
SSAN	29.4238	86.729	54.53	0.33	1.90	0.07	42
SUKT	27.7057	85.7611	45.95	0.21	1.75	0.07	12
TASH	27.7492	89.7309	71.57	0.18	1.64	0.05	4
THAK	27.5996	85.5566	37.53	0.29	1.91	0.09	8
TNC	25.029	98.52	43.00	0.27	1.43	0.07	58
TUML	27.3208	87.195	44.42	0.22	1.44	0.07	13
XIXI	28.7409	85.6904	46.38	0.66	1.85	0.08	16

YALA	28.4043	86.1133	57.58	0.30	1.96	0.06	21

5.3: DISCUSSION

The results show significant variation in the crustal thickness that increases from 35-40 km in the southern plains of Nepal and adjoining regions in the gangatic plains to 76-81 km in the Indus-Tsangpo Suture Zone and Eastern Trans-Himalaya in the northern belts of the Himalayan-Tibetan orogen.

The stacks of receiver function show a number of converted phases. The most pronounced phase corresponds to the moho, the surface which separates the high velocity in the mantle from the slower ones in the Indian continental crust. The base of the Indian crust is well defined by the receiver function analysis in terms of moho depth and validates the widely accepted opinion that lower Indian crust underplates the southern Tibetan plateau.

The receiver functions show an azimuthal dependence which might be due to lateral variation of the stations. A number of features in the observed receiver functions including strong energy in the transverse component and polarity reversals on the later phases of the radial component suggest an anisotropic layer or dipping structure underneath the stations in Nepal which might have continued to southern Tibet. A strong seismic anisotropy at the base of the Himalaya resulting from the shear process might be responsible for the slip causing great earthquakes in the Himalayan region (Schulte-Pelkum et al., 2005) like the recent 7.8 Magnitude earthquake in Nepal. The positive amplitude arrival seen at the southern Nepal stations at around

40 km depth suggest a lower velocity layer in the lower crust which probably consists of felsic materials made up of lighter elements.

Some receiver functions show an earlier arrival of the converted phase in the Lesser Himalayan region (for example station YALA with first conversion at ~4 seconds) which imply an uncharacteristically thin crust and which is inconsistent with the previous geophysical studies in the region (Gupta and Biswas, 2000). This could be a result of the conversion at decollement surface along which the Indian plate underthrusts the Tibetan plateau as suggested by (Mitra et al., 2005)

To summarize, the measurements of crustal thickness and Vp/Vs ratio across Himalaya and southern Tibet, in general, are consistent with the previous geophysical studies (Zhao et al., 1993; Alsdorf et al., 1998). However, our results include some receiver function, for which the primary P to S conversion do not represent the moho depth and thus require further investigation. Receiver function method has already been proved a successful technique in studying the crustal velocity structures and provides insight into many mysteries that lies underneath us in the crust and mantle.

References

Alsdorf, D., Brown, L., Nelson, K.D., Makovsky, Y., Klemperer, S., Zhao, W., 1998. Crustal deformation of the Lhasa terrane, Tibet plateau from Project INDEPTH deep seismic reflection profiles. Tectonics 17, 501–519. doi:10.1029/98TC01315

Bale, R., Gratacos, B., Mattocks, B., Roche, S., Poplavskii, K., Li, X., 2009. Shear wave splitting applications for fracture analysis and improved imaging: some onshore examples. First Break 27.

Bracewell, R.N., 1986. The Fourier transform and its applications, 2. ed., rev. ed, McGraw-Hill series in electrical engineering. McGraw-Hill, New York.

Crotwell, H.P., Owens, T.J., Ritsema, J., 1999. The TauP Toolkit: Flexible Seismic Travel-time and Ray-path Utilities. Seismol. Res. Lett. 70, 154–160. doi:10.1785/gssrl.70.2.154

Gansser, A., 1964. Geology of the Himalayas. Interscience, London.

Gupta, A.B.D., Biswas, A.K., 2000. Geology of Assam. Geological Society of India

Gupta, H.K., Narain, H., 1967. Crustal structure in the Himalayan and Tibet Plateau region from surface wave dispersion. Bull. Seismol. Soc. Am. 57, 235–248.

Heim, A., Gansser, A., 1939. Central Himalaya Geological observations of the Swiss expedition 1936. Gebrüder Fretz, Zürich.

Kearey, P., Klepeis, K.A., Vine, F.J., 2009. Global tectonics. Wiley-Blackwell, Chichester, West Sussex; Hoboken, NJ.

Kikuchi, M., Kanamori, H., 1982. Inversion of complex body waves. Bull. Seismol. Soc. Am. 72, 491–506.

Kosarian, M., 2006. Lithospheric Structure of North Africa and Western Eurasia. ProQuest.

Langston, C.A., 1979. Structure under Mount Rainier, Washington, inferred from teleseismic body waves. J. Geophys. Res. Solid Earth 84, 4749–4762. doi:10.1029/JB084iB09p04749

Langston, C.A., 1977. The effect of planar dipping structure on source and receiver responses for constant ray parameter. Bull. Seismol. Soc. Am. 67, 1029–1050.

Ligorría, J.P., Ammon, C.J., 1999. Iterative deconvolution and receiver-function estimation. Bull. Seismol. Soc. Am. 89, 1395–1400.

Liu, G., Einsele, G., 1994. Sedimentary history of the Tethyan basin in the Tibetan Himalayas. Geol. Rundsch. 83, 32–61. doi:10.1007/BF00211893

Molnar, P., 1984. STRUCTURE AND TECTONICS OF THE HIMALAYA: Constraints and Implications of Geophysical Data. Annu. Rev. Earth Planet. Sci. 12, 489. doi:10.1146/annurev.ea.12.050184.002421

Monsalve, G., Sheehan, A., Rowe, C., Rajaure, S., 2008. Seismic structure of the crust and the upper mantle beneath the Himalayas: Evidence for eclogitization of lower crustal rocks in the Indian Plate. J. Geophys. Res. Solid Earth 113, B08315. doi:10.1029/2007JB005424

Nábělek, J., Hetényi, G., Vergne, J., Sapkota, S., Kafle, B., Jiang, M., Su, H., Chen, J., Huang, B.-S., Team, the H.-C., 2009. Underplating in the Himalaya-Tibet Collision Zone Revealed by the Hi-CLIMB Experiment. Science 325, 1371–1374. doi:10.1126/science.1167719

Özalaybey, S., Savage, M.K., Sheehan, A.F., Louie, J.N., Brune, J.N., 1997. Shear-wave velocity structure in the northern Basin and Range province from the combined analysis of receiver functions and surface waves. Bull. Seismol. Soc. Am. 87, 183–199.

Rob W. Clayton and Ralph A. Wiggins, 1976. Source shape estimation and deconvolution of teleseismic bodywaves. Geophys. J. R. Astron. Soc. 47, 151–177. doi:10.1111/j.1365-246X.1976.tb01267.x

Schulte-Pelkum, V., Monsalve, G., Sheehan, A., Pandey, M.R., Sapkota, S., Bilham, R., Wu, F., 2005. Imaging the Indian subcontinent beneath the Himalaya. Nature 435, 1222–1225. doi:10.1038/nature03678

Seeber, L., Armbruster, J.G., Quittmeyer, R.C., 1981. Seismicity and Continental Subduction in the Himalayan Arc, in: Gupta, H.K., Delany, F.M. (Eds.), Zagros Hindu Kush Himalaya Geodynamic Evolution. American Geophysical Union, pp. 215–242.

Sheehan, A.F., Wu, F.T., Bilham, R., Blume, F., Monsalve, G., Bendick, R., Gilbert, H., de La Torre, T., Schulte-Pelkum, V., Wilson, C.K., Huang, G.C., Pandey, M.R., Liu, H.B., 2002. Himalayan Nepal Tibet Broadband Seismic Experiment (HIMNT). AGU Fall Meet. Abstr. 61, 11.

Sorkhabi, R.B., Macfarlane, A., 1999. Himalaya and Tibet: Mountain roots to mountain tops, in: Special Paper 328: Himalaya and Tibet: Mountain Roots to Mountain Tops. Geological Society of America, pp. 1–7.

Stein, S., Wysession, M., 2002. An Introduction to Seismology, Earthquakes and Earth Structure, 1 edition. ed. Wiley-Blackwell, Malden, MA.

Tandon, A.N., Dube, R.K., 1973. A study of the crustal structure beneath the Himalayas from body waves. Pure Appl. Geophys. 111, 2207–2215. doi:10.1007/BF00940871

Velasco, A.A., Gee, V.L., Rowe, C., Grujic, D., Hollister, L.S., Hernandez, D., Miller, K.C., Tobgay, T., Fort, M., Harder, S., 2007. Using Small, Temporary Seismic Networks for Investigating Tectonic Deformation: Brittle Deformation and Evidence for Strike-Slip Faulting in Bhutan. Seismol. Res. Lett. 78, 446–453. doi:10.1785/gssrl.78.4.446

Windley, B.F., 1995. The Evolving Continents, 3 edition. ed. Wiley, Chichester ; New York.

Zhao, W., Nelson, K.D., Che, J., Quo, J., Lu, D., Wu, C., Liu, X., 1993. Deep seismic reflection evidence for continental underthrusting beneath southern Tibet. Nature 366, 557–559. doi:10.1038/366557a0

Zhu, L., Kanamori, H., 2000. Moho depth variation in southern California from teleseismic receiver functions. J. Geophys. Res. Solid Earth 105, 2969–2980. doi:10.1029/1999JB900322

Vita

Arjun Neupane was born in the city of Bharatpur in Nepal. He grew up in Nepal and completed his Bachelors from Birendra Multiple Campus, Bharatpur and Masters from St. Xavier's College, Kathmandu, both in Physics. He joined UTEP in the fall of 2013.

Arjun came to UTEP as a graduate student and a teaching assistant in the Department of Physics. He started working under Dr. Aaron Velasco in the Department of Geological Sciences from the spring of 2014. He has been working on the method of P wave receiver function analysis to study the crustal structure beneath the Himalayas. After completing this work, Arjun plans to continue working on Seismology for his PhD degree.

Permanent email address: arjunneupane@gmail.com

This thesis was typed by Arjun Sharma Neupane